Common features of neural progenitor cells and cortical organization revealed by single cell transcriptome analyses of ferret cortical development

Merve Bilgic

Table of Contents

ABSTRACT

The cerebral cortex underlies the cognitive abilities of mammals, including humans, and forms by sequential generation of a diversity of neuron and glia types from neural progenitor cells (NPCs). The diversity of neural stem cells is a fundamental characteristic of cerebral cortex development in Gyrencephalic mammals, including Primates and Carnivora. Among these species, ferrets have emerged as a valuable model for mechanistic studies due to their cortical similarities to humans. However, the information on molecular and cellular features of their NPCs remains fragmented. Thus, understanding the cellular diversity and transcriptomic profiles of RG subtypes in developing ferret brain is important.

In this study, we conducted single-cell transcriptome analyses throughout various developmental stages in the ferret cortex to investigate the cellular diversity and temporal trajectory of NPC. Our comparative analyses revealed a conserved diversity and temporal trajectory of NPC between humans and ferrets. We identified remarkable conservation of RG cell types at the transcriptome and morphological level between ferrets and humans. In particular, we examined the generation of truncated radial glia (tRG), a human-enriched RG subtype previously described in humans (Nowakowski *et al*, 2016). Furthermore, employing a combination of *in silico* and *in vivo* analyses, we identified that tRG differentiate into both ependymal and astrogenic cells. Our comparative analyses with human datasets suggested a similar fate for tRG in humans. Furthermore, the timelapse imaging and slice culture experiments proposed that tRG emerge from asymmetric divisions of RG and that BMP signaling might play role in its maintenance.

Through transcriptomic comparison, our findings indicate that tRG play a pivotal role in the formation of adult ventricles, which ultimately provides the architectural foundation for brain expansion. These insights contribute to our understanding of cortical development in ferrets and humans, further reinforcing the significance of ferrets as a valuable model system for investigating Gyrencephalic brain features.

The comprehensive dataset generated in this study contains multiple developmental stages, providing a crucial resource for future investigations in cortical brain development. This research not only enhances our understanding of cortical development in ferrets but also holds implications for comparative studies across species. Our findings demonstrate that ferrets serve as a valuable model system for studying Gyrencephalic brain features shared between ferrets and humans, which are otherwise challenging to explore in humans due to ethical and practical limitations.

Chapter 1

INTRODUCTION

1.1. Development of Gyrencephalic cerebral cortex.

1.1.1. Generation of cellular diversity during cortical brain development.

The cerebral cortex occupies the largest region of the mammalian brain and plays a central role in behavior and cognition, such as memory and reasoning. During brain development, the cortex is generated in an inside-out manner from two major types of neural progenitor cells (NPC); radial glial (RG) cells and intermediate progenitor cells (IPC). RG cells are localized in the germinal zones near lateral ventricles and act as neural stem cells during brain development. They present epithelial-like characteristics such as apical and basal radial fibers connecting both ventral and dorsal surfaces of the developing neocortex (Figure 1.1.1; Taverna *et al*, 2014; Fernández *et al*, 2016). These fibers serve as a scaffold to neurons, facilitating their migration towards basal side of the cortex.

RG cells achieve neurogenesis by dividing asymmetrically on the ventricular surface (VS); while one daughter cell becomes either a neuron or an IP, the other one self-renews. IPC lose epithelial-like features and apical junctions, then migrate basally to form the subventricular zone (SVZ), where they produce two neurons by dividing only once (Figure 1.1.1; Noctor *et al*, 2004). Gliogenesis then follows neurogenesis at later stages where NPC produce astrocytes, oligodendrocytes and ependymal cells. This temporally regulated developmental events constructs a six-layered neocortex where neurons born from early-stage progenitors migrate and form deep-layers in the cortical plate, and late born-neurons end up as upper-layer neurons in the maturating and adult brains (Frantz & McConnell, 1996).

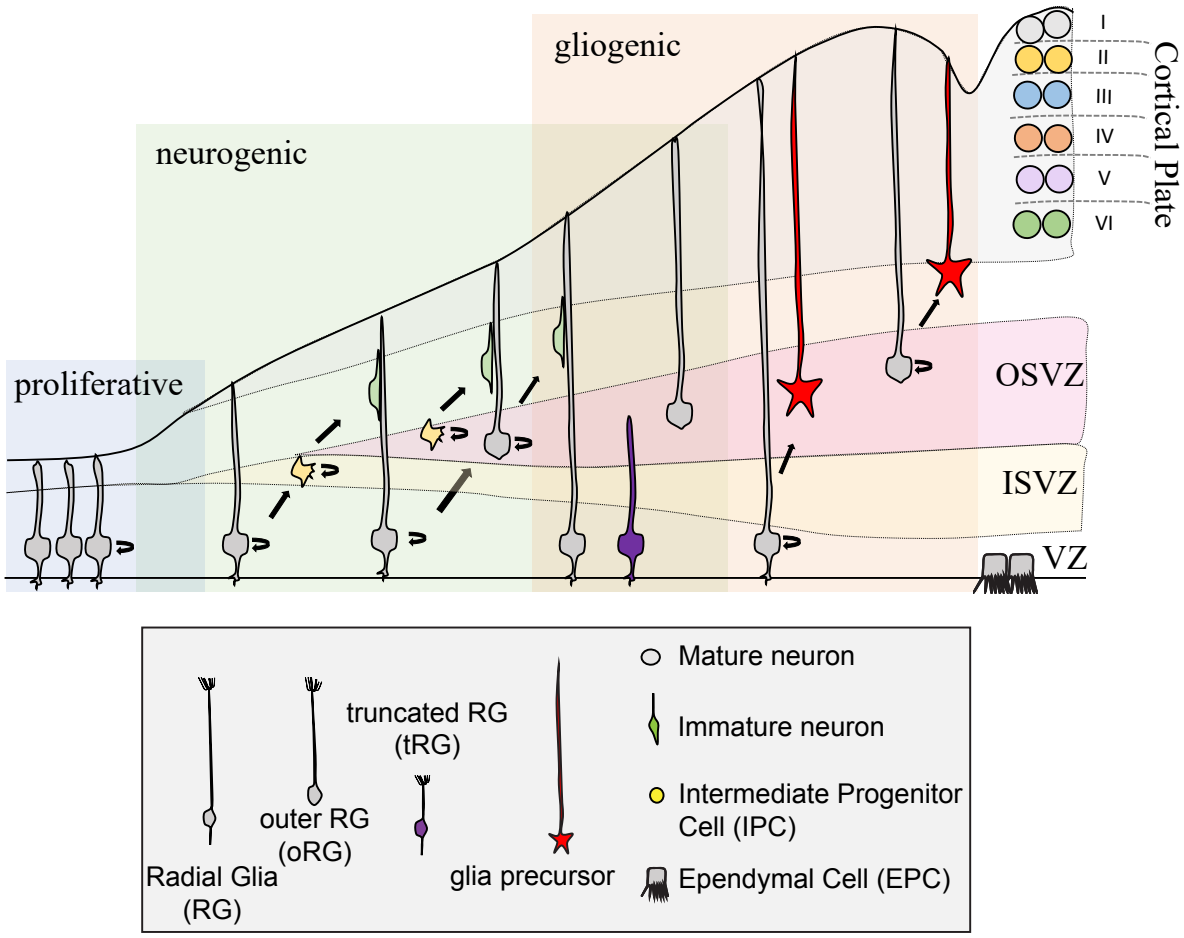

Figure 1.1.1 Development of cerebral cortex.
Schematic representing cortical development and emergence of diverse neural progenitors in humans and ferrets. Progenitors sequentially generate DL- and subsequent UL-neurons, and finally glial cells, and form ependymal cells. RG and oRG have been morphologically and positionally identified in both humans and ferrets while tRG have been only reported in humans. VZ, ventricular zone; ISVZ, inner subventricular zone; OSVZ, outer subventricular zone; IZ, intermediate zone; DL, deep layer; UL, upper layer; CP, cortical plate; NEP cell, neuroepithelial cell; Mn, migrating neuron; and EP cell, ependymal cell.

1.1.2. Hallmarks of the mammalian brain evolution in developing brains.

The size of neocortex is a major determinant for the mammalian brain complexity and its expansion during evolution reflects higher brain functions, such as perception, conscious thoughts, and decision-making (Roth, 2015; Dicke & Roth, 2016). The increase of neocortical size is accompanied with the formation of convolutions in gyrencephalic species accounting for greater surface area of cortical neurons, which allows the brain to overcome space limitations within the skull (Figure 1.1.2).

The increase of cortical size has a correlation with increased numbers of neurons and glia (Haug, 1987; Herculano-Houzel *et al*, 2006), two major types of cells forming the adult brain. A major driving force of this increase is changes occurring at the level of neural progenitor cells (NPCs) during mammalian brain evolution. Such changes include the emergence of new types of NPC and their increased proliferation capacity (Smart *et al*, 2002; Hansen *et al*, 2010; Betizeau *et al*, 2013; Shitamukai *et al*, 2011). The most studied novel RG type is named outer radial glia (oRG), dividing outside of ventricular zone (VZ), and retaining only elongated basal fiber without apical junctions and anchoring to the VS, has emerged in primates and carnivores (Figure 1.1.1; Hansen *et al*, 2010; Fietz *et al*, 2010; Reillo *et al*, 2011). This progenitor cell population is expanded to form the outer SVZ (OSVZ) in complex brains such as primates and carnivores including ferret, while rodents do not form the OSVZ (Figure 1.1.2; Smart *et al*, 2002). The oRG holds a significant contribution to the increase of neuronal and glial output (Rash *et al*, 2019; Huang *et al*, 2020). Several studies suggested that oRG contribute to the expansion and folding of the cerebral cortex, hence, to higher brain functions. However, molecular mechanisms regulating their generation, maintenance, and proliferation at a distance from ventricles remains unclear, partly because the use of mice as a model organism for these human-enriched cell types is restricted.

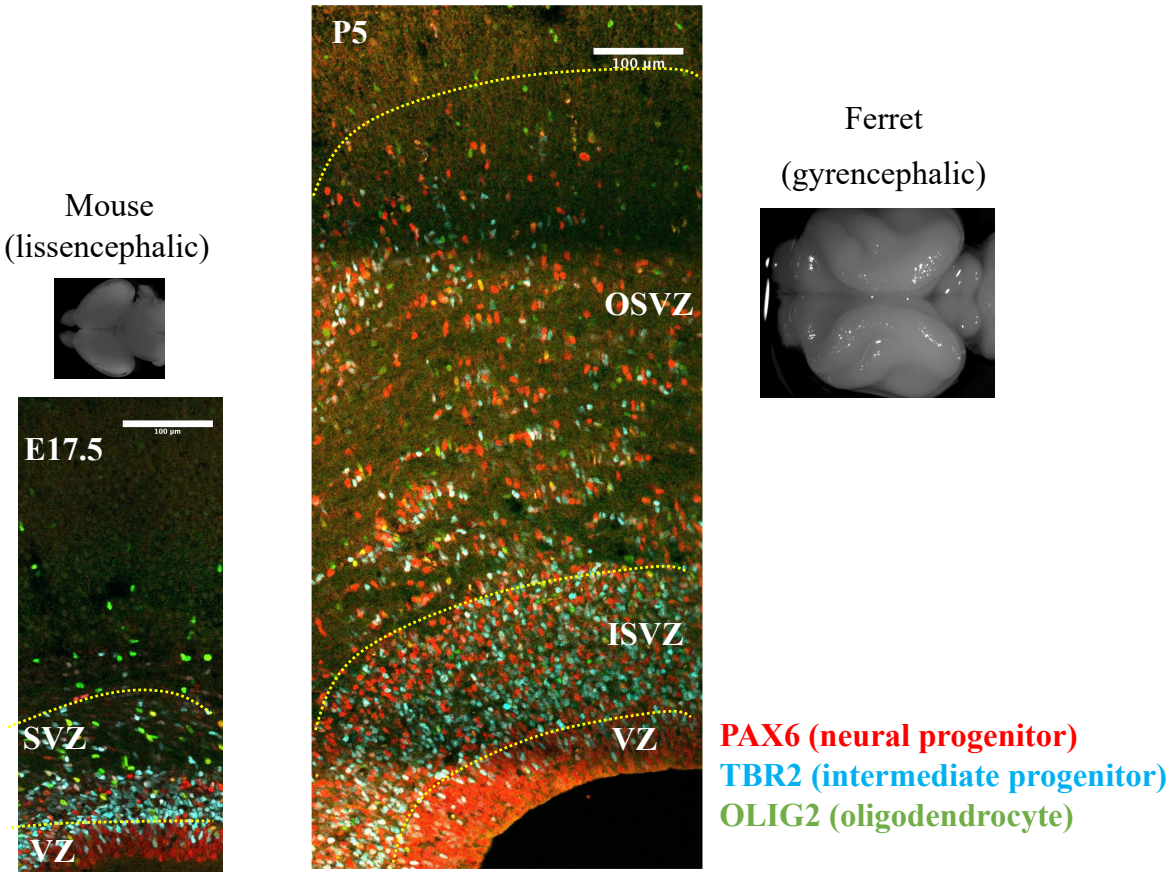

Figure 1.1.2. The evolutionary expansion of neocortex: emergence of OSVZ and cortical folding. The representation of the emergence and expansion of the Outer Subventricular Zone (OSVZ) in coronal sections of the cerebral cortex at corresponding developmental stages in mice and ferrets. The sections were immunostained with PAX6, TBR2, and OLIG2 markers to visualize neural progenitors, intermediate progenitors, and oligodendrocytes, respectively. Brain images show the development of cortical folding in ferrets, contrasting with the smooth cortex observed in mice.

1.2. Ferrets as a model for studying Gyrencephalic brain development.

Ferrets, *Mustela putorius furo*, are Gyrencephalic carnivores characterized with an expanded and folded cortex, and a diversity of NPCs during its brain development. Ferrets have initially captivated neuroscientists as an attractive model for investigating the visual and auditory circuits due to their prolonged maturation into postnatal stages, distinguishing ferrets from mice and humans, and thereby making ferrets a convenient model for experiments (Kelly *et al*, 1986; Jackson *et al*, 1989; Dehay *et al*, 2015; Gilardi & Kalebic, 2021). In the neurodevelopment field, ferrets present a unique opportunity to examine all aspects of developmental processes - from neurogenesis and migration to neuronal differentiation and circuit formation – extending beyond birth, and thus rendering ferrets more available to manipulation (McConnell, 1985).

1.2.1. Conservation of radial glia (RG) cell types between ferrets and humans.

Ferrets have been shown to emerge human-enriched RG cell types during cortical development (Reillo & Borrell, 2012; Borrell & Reillo, 2012). Live imaging analyses on cortical slice culture of ferrets have revealed the distinct characteristics of ferret oRG and IPCs within the OSVZ, including cell division dynamics. These studies have shown that ferret oRG exhibit higher proliferative capacity when compared to their counterparts in rodents (Gertz *et al*, 2014). This elevated proliferation capacity contributes to an increased production of both neurons and glial cells within the developing cortex. Yet, the molecular features and signaling pathways governing these processes and distinguishing different RG subtypes in ferrets remained less understood. Moreover, elucidating the comparison in gene expression profiles between ferrets and primates during cortical development is pivotal for comprehensive aspects on both shared and distinct features of RG cell types. These revelations could not only extend our knowledge on cortical development, but also potentially contribute to our comprehension of neurodevelopmental disorders.

1.2.2. The novel type of human RG with an undefined function: truncated radial glia (tRG).

Recent human studies have reported another novel type of RG, termed truncated RG (tRG), with its unique morphology of a short basal fiber (Nowakowski *et al*, 2016; DeAzevedo *et al*, 2003). tRG has been demonstrated to emerge in the mid-neurogenic stages of human developing brain (Nowakowski *et al*, 2016). In contrast to oRG, tRG remains in the VZ during late neurogenesis and dominates the VZ (Figure 1.1.1). In humans, molecular features of tRG have been revealed by single cell transcriptome studies (Nowakowski *et al*, 2016; Nowakowski *et al*. 2017).

Despite the progress in characterizing tRG cells by *in silico* and *in vivo* studies in terms of their transcriptomic and morphological properties, their precise function, mechanisms how tRG emerge in developing brain and whether it is a common cell type to Gyrencephalic species remain undetermined. Understanding the properties and functions of tRG might provide valuable insights into human brain development and potential related neurodevelopmental diseases.

1.2.3. Advantages and limitations of ferrets as a model.

Ferrets have been used as model animal to study the cortical development since about 30 years. Ferrets' neuroanatomical similarities with primates and experimental advantages make them an ideal candidate for investigating brain development and neural progenitor cell dynamics.

The relatively short gestation period spanning about 41 days and the postnatal development make ferrets a practical model animal to study different stages of cortical development of Gyrencephalic species, including neurogenesis, gliogenesis, migration and circuit formation. In addition, ferrets are experimentally manipulable, such as genetic modifications and *in utero* electroporation for a gene delivery (Borrell, 2010; Kawasaki *et al*, 2012), allowing researchers to trace cell lineages *in vivo*, and to study specific molecular mechanisms underlying cortical development.

Ferrets offer novel developmental aspects unique to Gyrencephalic species, that cannot be fully understood by mice studies. An illustration that exemplifies this idea can be observed when comparing the differenct phenotypes in mice and ferrets in functional studies, including following the removal of a shared gene from RG cells. The deletion of LGN, a protein involved in the spindle orientation in NPCs (Konno *et al*, 2007), has been shown to induce apical divisions with oblique cleavage plane orientations within the mouse cortex, leading to a formation of self-renewing oRG-like cells showing a morphological resemblance to Gyrencephalic oRG (Shitamukai *et al*, 2011). Although this and other studies on mice (Kawaue *et al*, 2019; Fujita *et al*, 2020) have proposed oblique divisions as a contributing mechanism for oRG formation, in mice with specific genotypes, the inheritance of basal process and the emergence of oRG-like cells did not influence the neuronal output (Konno *et al*, 2007). These studies implies that the forced increase of oRG alone is not essential to enhance the neuronal production and subsequently, the cortical size in mice. These studies illustrated here thus highlight that rodents provide molecular basis crucial to understand cellular dynamics. However, they also suggest the necessity of selecting model animals that naturally generate high quantities of these specific cell types. This is crucial to achieve a deeper understanding of cellular dynamics involved. Additionally, it emphasizes the need for extensive molecular comparisons of these cell types across species to validate their cellular functions.

To achieve these aspects, the utilization of single-cell transcriptomics emerges as a powerful approach. While transcriptomic investigations have been extensively carried out in humans (Herring *et al*, 2022; Bhaduri et al, 2020, 2021; Huang et al, 2020; Johnson et al, 2015; Liu et al, 2017; Polioudakis et al, 2019; Pollen et al, 2015; Zhong et al, 2018), the availability of transcriptomic datasets focused on ferrets remains limited.

1.3. Aims

1) Characterization of different neural progenitor subtypes in the ferret cortex.
2) Comparison of the cortical brain development between ferrets and human in terms of cellular diversity of RG subtypes and their transcriptomic profiles.
3) Do ferrets develop human-like RG, and can they be used as a model system to study these cells?
4) How does the ferret/primate-specific RG form and what is their role in Gyrencephalic species?

To answer these questions and to provide a comprehensive dataset spanning various developmental stages, we have performed single-cell transcriptome analyses in a temporal series of cortical development in ferrets on an improved genomic background. We discovered that tRG emerges in developing ferret brain and revealed the conservation of RG cell types at transcriptome levels between ferrets and humans, making ferrets a valuable model for studying common Gyrencephalic brain features during development, which are otherwise difficult to address in humans due to ethical and practical issues, as well as in mice due to limitations mentioned earlier.

Chapter 2

MATERIAL and METHODS

Breeding, Maintenance of Ferrets, and Preparation of Brain Tissues

Pregnant ferrets were obtained either by a purchase from Marshall Bioresources or by breeding them in the animal facility of RIKEN Center for Biosystems Dynamics Research under the license given from the provider. The maintenance and experimental procedures of animals were performed in accordance with the legal and ethical regulations of RIKEN Center for Biosystems Dynamics Research.

Ferret pups are born at day 41 or 42 of gestation. The day of birth was counted as postnatal day 0 (P0).

Pregnant ferrets or their pups were kept under deep anesthesia with isoflurane during the procedure of a transcardial perfusion for fixation of tissues.

***In Utero* and Postnatal Electroporation**

In utero electroporation (IUE) and postnatal electroporation in ferrets was performed as described previously with modifications (IUE: Kawasaki *et al*, 2012; Asuka *et al*, 2013; Tsunekawa *et al*, 2016; postnatal: Borrell, 2010). Briefly, pregnant ferrets or ferret pups were anesthetized with isoflurane at indicated stages of the development. 3 µl of plasmid DNA solution was injected into the lateral ventricle. In the case of pups, the location of lateral ventricles was visualized with the transmitted light delivered through an optical fiber cable. Upon injection, embryo or pup was placed between the paddles of electrodes, and was applied a voltage pulse of 45V or 60V, respectively, at the duration from 100 milliseconds to 900 milliseconds (100,0 Pon and 1000,0 Poff) for 10 times (CUY21 electroporator, Nepa Gene).

Plasmids and Developmental Timepoints of Plasmid Delivery

For scRNA-seq samples, the enrichment of neural progenitor cell populations at the expense of differentiated neurons was achieved in "AG" samples by isolating these cells through AzamiGreen expression under the control of *HES5* promoter (mouse), which is active in the undifferentiated neural progenitor cells. The plasmid of pLR5-Hes5-d2-AzamiGreen (0.5 µg/µl; Hes5 promoter was gifted from Kageyama Laboratory; Ohtsuka et al., 2006) was included in the DNA solution mix, which was electroporated at E30 for E40, or at E34 for postnatal samples. Among them, for P1 and P10 samples, pPB-LR5-mCherry (0.5 µg/µl) was also included in the DNA solution to visualize the electroporation efficiency.

A sparse labeling was performed for a detailed imaging of individual cell lineages on vibratome-cut thick cortical sections. The sparse labeling system included an EGFP expression vector under the control of Cre (0.5 µg/µl of pPB-LR5-floxstop-EGFP and 1 or 10 ng/µl of Cre-expressing plasmid for P0 or P5 samples, respectively).

For all electroporation experiments, a stabilized expression of transgenes was generated using hyperactive piggyBac transposase system that enables the integration of expression vectors into the genome for a stable expression (Yusa *et al*, 2011). The plasmid of pCAX-hyPBase (0.5 µg/µl) was mixed in the DNA solution. Moreover, Fast Green solution (0.1 mg/ml; Wako Pure Chemical Industries) was added into the freshly prepared mixture of plasmid DNA to visualize the injected area.

For *in situ* hybridization probes, PCR product was inserted into pCR-BluntII-TOPO for cloning and sequencing.

Probe Preparation
Primer3 ver 0.4.0 software was utilized to design primers for PCR, specifically targeting the genes of interest. Trizol was employed to collect total RNA from embryonic ferret brain. The Prime Script 1st strand cDNA synthesis kit (Takara) was utilized to generate cDNA from the total RNA, following the manufacturer's recommended procedure. The target cDNA was inserted into the pCR-TOPOII-Blunt plasmid, utilizing M13F or M13R primers. Subsequently, anti-sense cRNA probes were produced through *in vitro* transcription, using the T7 promoter.

***In situ* Hybridization**
ISH was performed as described previously, with modifications (Mashiko *et al*, 2012). A transcardial perfusion with cold PBS, followed by 4% PFA in Phosphate-buffered saline (PBS) was performed on ferret pups. Collected brains from ferret embryos or pups were fixed with 4% PFA in 0.1M phosphate buffer (PB, pH 7.4). The fixed brains were then immersed in a solution of 30% sucrose in 0.1M PB for a minimum of one day and stored at -80°C until further ISH processing. The frozen brains were sectioned in the coronal plane at a thickness of 25 µm using Cryostat (CM3050S Leica Microsystems). The sections were mounted onto slides and post-fixed with 4% PFA in 0.1M PB, followed by treatment with proteinase K (Roche). Next, the sections were subjected to overnight hybridization at 72°C using digoxigenin (DIG)-labeled probes in a hybridization solution. Subsequently, the sections were washed, blocked with donkey serum, and incubated with pre-absorbed DIG antibody conjugated to alkaline phosphatase for 2 hours at room temperature. The color development process was carried out using a solution containing NBT/BCIP (Roche).

Immunohistology and Confocal Imaging
Embryonic or pup ferret brains were extracted and fixed for 1 or 2 overnights, respectively, in a 1% PFA solution prepared in 0.1M PB at 4℃. P35 ferrets underwent transcardial perfusion with cold PBS, followed by 4% PFA. The collected brains were then post-fixed with 1% PFA. Following fixation, brains or cortical tissue slices were equilibrated overnight in 25% sucrose before being embedded in O.C.T. compound (TissueTek, Sakura) and frozen in liquid nitrogen. The frozen samples were subsequently stored at -80℃ until coronal sectioning, which was performed using a cryostat (CM3050S Leica Microsystems) to obtain 12µm sections. Once equilibrated at room temperature, the sections were washed in PBS with 0.1% Tween (PBST) and then treated with an antigen retrieval solution, HistoVT one (Nacalai Tesque), diluted 10 times in milliQ water, at 70℃ for 20 minutes. The sections were then blocked for 1 hour at room temperature (RT) using a blocking solution consisting of PBS with 2% Triton-X100 and 2% normal donkey serum (Sigma). Subsequently, the sections were incubated overnight at 4℃ with the primary antibody, appropriately diluted in the blocking solution. After three washes in PBST, the sections were incubated with suitable fluorescence-conjugated secondary antibodies (1:500) and 4',6-diamidino-2-phenylindole (DAPI, 1:1,000) for 1 hour at room temperature. Following another round of washing, the sections were mounted using PermaFluor solution (Thermo Fisher Scientific).
The immunostaining of thick ferret brain sections (200 µm) was conducted following the previously reported method (Tsunekawa et al., 2016). Initially, ferret brains were fixed in 1% PFA, washed overnight at 4℃ in PB, and then embedded in 4% low-melting agarose (UltraPure LMP agarose, Thermo Fisher Scientific). Coronal brain slices with a thickness of 200 µm were obtained

by sectioning the embedded brains using a vibratome (LinerSlicer, DOSAKA EM) on ice. The floating sections were washed three times with PBST, followed by treatment with the blocking solution for 1 hour at room temperature (RT). Subsequently, the sections were incubated with primary antibodies for 5 or 6 overnights at 4℃ under shaking. After washing with PBST, the sections were treated with secondary antibodies for 5 or 6 overnights at 4℃ under shaking. Following a final round of washing, the brain slices were mounted using CUBIC solution 2 to achieve transparency. Fluorescent images were acquired using an FV1000 confocal microscope (Olympus, Japan). The somatosensory cortices were captured using either a 20X or 100X objective lens. In cases where the 100X objective lens was used, z-stacks of confocal images were taken with an optical slice thickness of 1.0 µm or 1.5 µm, and MAX-projection images obtained by FiJi software are presented.

Evaluation of Immunolabeled Cell Number and Statistical Analysis

150 µm of width regions of interests (ROIs) were selected on images of immunolabeled sections. The counts of immunolabeled cells within these ROIs were manually conducted using the "cell counter" tool in FiJi software (Schindelin *et al*, 2012). The VZ was identified based on cell density visualized by DAPI staining and the measured thickness from the ventricular surface at indicated stages (100 µm at P5, 70 µm at P10). The proportions of immunolabeled cells positive for different markers were calculated by summing the data counted within all ROIs. Data obtained from the lateral cortices of somatosensory area were averaged from 2 to 3 sections.

For CRYAB-positive cells, only cells with visible nuclei by DAPI were counted. The numbers of positive cells were counted from two or three different animals.

Statistical significance was assessed using the Wilcoxon test, and data from each section were considered as n = 1.

Single Cell Isolation and Sorting of Azamigreen-expressing Cells

A cell suspension was prepared as reported previously (Wu *et al*, 2022) with some modifications.

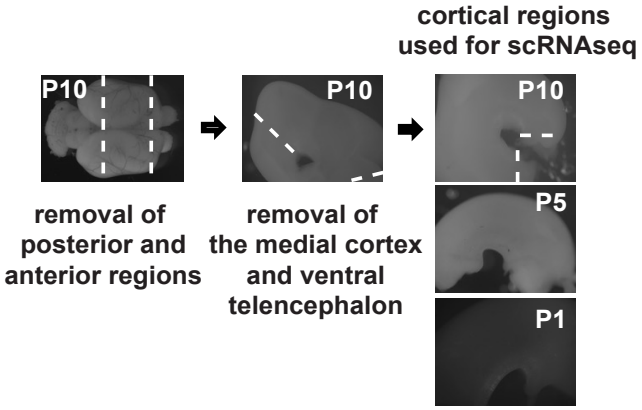

Brains were collected at the indicated stages and transferred to ice-cold dissection Dulbecco's Modified Eagle Medium (DMEM) F12. The meninges were removed, and the cortical area was dissected from embryonic or postnatal cortices using a 15°ophthalmic knife under a dissection microscope. The sliced tissues were then dissociated through enzymatic digestion using papain at 37℃ for 30-45 minutes in ice-cold Hank's Balanced Salt Solution (HBSS) (-) with EDTA (0.1 M). The dissociated cells were centrifuged at 1000xg for 5 minutes to remove papain, washed with PBS, and resuspended either in 0.375% BSA/HBSS (-) or in the sorting buffer (DMEM F12 + GlutamaX (Thermo Fisher), 0.1% Penicillin/Streptomycin (Millipore), 20 ng/ml human basic FGF (Peprotech), 1xB27 RA- (Gibco)) for cell sorting (described below). The homogenous cell suspension was filtered through a 35 µm strainer (Falcon).

To concentrate neural progenitor cell (NPC) populations while minimizing mature neurons, two methods were employed for each sample, except for E25, where cells were collected from the entire somatosensory area:
1) "T" samples: The cortical plate (CP) of cortical sections was dissected out, and a portion of the intermediate zone (IZ) might have been included in the discarded region.
2) "AG" samples: Brains collected at the specified stages were electroporated *in utero* with an azamiGreen (AG)-expression vector under the control of the Hes5 promoter. This method allows AG expression only in NPCs by incorporating a degradation signal "d2" in the vector, leading to the degradation of AG protein in HES5-negative differentiating progeny. Only "AG" samples underwent cell sorting, and the dissociated cells obtained as described above were sorted for azamigreen-positive cells using a SH800 cell sorter (SONY) in a 0.375% BSA/HBSS (-) solution. Cell survival and cell numbers were quantified using the Countess or Countess II (Invitrogen) before applying single-cell isolation with the 10x v2 Chromium kit.
Samples from the same developmental stage, except for the P10 "T" sample, were born from the same mother and collected by applying either of the above methods on the same day and processed in parallel.

Library Preparation and scRNA-sequencing
10x v2 Chromium was performed on dissociated single cells according to the manufacturer's protocol. Cell suspensions were diluted for an appropriate concentration to obtain 3,000 cells per channel of a 10X microfluidic chip device and were then loaded on the 10X Chromium chips accordingly to the manufacturer's instructions.
Total cDNA integrity and quality were assessed with Agilent 2100 Bioanalyzer.
Libraries were sequenced on the HiSeq PE Rapid Cluster Kit v2 (Illumina), or the TruSeq PE Cluster Kit v3-cBot-HS, to obtain paired-end 26 nt (Read 1)-98 nt (Read 2) reads.

Alignment and Raw Processing of Data
Fastq files were obtained from individual samples and were processed using Cell Ranger pipeline v2. Alignment was done using "Cell Ranger count" function with default parameters accordingly to manufacturer's instructions to map reads to the ferret reference (MPF_Kobe 2.0.27).

Mapping Statistics generated by Cell Ranger v.2.0.2

Sample name	Estimated. Number. of.Cells	Mean. Reads. per.Cell	Median. Genes. per.Cell	Number.of. Reads	Valid. Barcodes	Reads.Mapped Confidently.to. Transcriptome	Reads.Mapped Confidently.to. Exonic.Regions	Reads.Mapped. Confidently.to. Intronic.Region	Reads.Mapped. Confidently. to.Intergenic. Regions	Reads. Mapped. Antisense. to.Gene	Sequencing. Saturation	Q30.Bases in.Barcod e	Q30.Bases. in.RNA.Rea d	Q30.Bases. in.Sample.I ndex	Q30.Bases. in.UMI	Fraction. Reads.in.C ells	Total. Genes. Detected	Median. UMI. Counts. per.Cell
E25	3,495	49,658	2,619	173,557,523	98.10%	60.30%	63.00%	18.40%	3.10%	9.20%	68.30%	97.30%	87.60%	96.60%	97.60%	92.60%	18,751	8,338
E34_AG	3,223	42,716	1,763	137,673,935	98.30%	58.20%	60.80%	23.00%	3.70%	8.20%	80.60%	97.30%	88.60%	96.70%	98.00%	94.00%	17,886	3,983
E34_T	2,265	47,465	2,195	107,508,876	98.20%	56.40%	59.20%	24.00%	3.60%	8.70%	75.80%	97.40%	88.30%	96.70%	97.80%	95.00%	17,838	5,863
E40_AG	1,103	51,662	2,233	56,983,319	98.10%	53.00%	55.60%	26.80%	3.90%	7.20%	69.60%	97.80%	86.00%	97.00%	97.80%	77.30%	17,367	5,747
E40_T	1,581	68,088	1,368	107,647,502	97.90%	51.00%	53.70%	31.30%	4.00%	7.10%	89.40%	97.60%	88.00%	96.70%	97.60%	95.00%	17,060	2,739
P1_AG	2,681	45,034	1,581	120,738,453	97.50%	51.40%	54.30%	28.40%	5.10%	7.70%	80.40%	97.70%	89.20%	96.80%	97.30%	86.00%	18,324	3,148
P1_T	3,647	58,287	1,062	212,575,114	97.50%	49.60%	52.40%	21.30%	3.80%	10.50%	84.00%	97.70%	87.60%	96.70%	97.30%	59.80%	18,417	1,904
P5_AG	2,431	47,437	1,517	115,320,578	97.20%	58.90%	61.40%	22.40%	4.00%	7.50%	80.70%	97.70%	86.50%	95.80%	97.80%	81.40%	19,265	3,469
P5_T	2,928	49,345	1,111	144,483,631	97.30%	60.70%	63.80%	14.90%	3.20%	11.00%	65.60%	97.70%	84.80%	97.00%	97.80%	28.60%	18,334	2,172
P10_AG	3,028	44,426	1,818	134,522,306	97.60%	58.30%	60.80%	22.10%	4.40%	7.30%	75.60%	97.70%	87.20%	96.70%	97.90%	84.60%	20,622	4,539
P10_T	3,935	51,462	799	202,506,773	97.60%	56.10%	58.50%	10.50%	2.40%	12.90%	77.90%	98.00%	87.20%	97.30%	97.70%	31.70%	18,450	1,428

Sequencing statistics data were generated by the Cell Ranger v.2.0.2 software of 10x Genomics using MusPutFur 2.60 (DDBJ DRA010274) as reference.

The raw data for each set of cells within a sample was obtained by cellranger count function and was read using Seurat "Read10X" function (Seurat v3.1.5) (Stuart *et al*, 2019), creating a matrix for unique molecular identified (UMI) counts of each gene within each cell.

For this study, we utilized an expanded reference gene annotation ferret genome. Briefly, to construct gene models, the Chromium Genome Reagent Kit v1 Chemistry was used to tag all

fragments derived from genomic DNA within a droplet (10x Genomics, Cat No. #PN-120126), and sequencing was performed with an Illumina HiSeq X to obtain paired-end 151 nt-long reads (Bilgic et al., 2023). The gene model construction under a collaboration with Kuraku Laboratory allowed for a successful alignment of sequences from long genomic DNAs, thereby enabling coverage of previously unconnected genomic regions in the NCBI database (NCBI Assembly ID: 286418, MusPutFur1.0).

	Reference	Estimated Number of Cell	Median Genes per Cell	Number of Reads	Reads Mapped to Transcriptome	Total Genes Detected	Median UMI Counts
E34_AG	NCBI	3,226	953	137,673,935	30.70%	14,562	2,153
E34_AG	This study	3,223	1,763	137,673,935	58.20%	17,886	3,983
E34_T	NCBI	2,260	1,182	107,508,876	29.90%	14,445	3,096
E34_T	This study	2,265	2,195	107,508,876	56.40%	17,838	5,863

For a comparison following the mapping process of our scRNAseq dataset with these two reference models, two of our samples were compared with the new and old models as indicated in the table. The new model improved the mapping rate and provided higher numbers of median UMI counts per cell.

The genome assembly and chromium linked-read sequences were deposited in the DNA Data Bank of Japan (DDBJ) under accession number DRA016867. The gene models are available from Figshare under the DOI: 10.6084/m9.figshare.12807032.

Filtering and Normalization

Filtering and normalization were performed using Seurat (v3.1.5) (Stuart *et al*, 2019). Briefly, each sample underwent filtering by removing low-quality cells with unique gene counts less than 200, and genes expressed in less than 3 cells (Seurat function "CreateSeuratObject"). Different samples were then merged using the Seurat "merge" function. Merged data was further subset by retaining cells with features (genes) over 200 and less than 5000. Raw UMI counts were then normalized using "LogNormalize" as normalization method, which divided reads by the total number of UMIs per cell, then multiplied by 10,000 (Seurat "NormalizeData" function). This resulted in a total of 30,234 cells and 19,492 genes: E25 (3486 cells), E34AG (3223 cells), E34T (2260 cells), E40AG (1102), E40T (1581 cells), P1AG (2681), P1T (3641), P5AG (2429), P5T (2926), P10AG (3010) and P10T (3895).

Single-cell Clustering and Visualization

Cell clustering was employed to the entire cell population after removing low-quality cells, using Seurat (v3.1.5) (Stuart *et al*, 2019). 2,000 highly variable genes were identified for downstream analyses using Seurat "FindVariableFeatures" function (selection.method = "vst"), which allowed the calculation of average expression and dispersion for each gene. The normalized data was then scaled using Seurat function "Scale Data" with default settings, which also allowed the regression of the batch.

Principal component analysis (PCA) was conducted on the scaled dataset using 2,000 variable genes to reduce dimensionality and 50 PCs were retained (Seurat "RunPCA" function). Clustering was performed using graph-based clustering approach ("Find Neighbors" function) using top 20

PCs. The selection of these PCSs was based on the standard deviation of PCs on the elbowplot created by Seurat function “ElbowPlot” and based on statistical significance calculated by JackStraw application.
In brief, cells are embedded in a k-nearest neighbor (KNN) graph based on the Euclidean distance in a PCA space. This KNN graph was then used to group cells on a shared nearest neighbor graph, considering the overlap between cells with similar gene expression patterns (Jaccard similarity). The cells were subsequently clustered using the Louvain algorithm implemented in Seurat “ClusterCells” function (resolution = 0.8, dims = 1:20).
Finally, the Seurat “RunUMAP” function was employed to generate a UMAP (Uniform Manifold Approximation and Projection) embedding. This resulted in cell clusters being separated in embedding space while preserving the balance between local and global structure.

Cluster Annotation
Cluster markers were obtained using the Seurat function "FindAllMarkers". Genes were considered as cluster markers if they showed at least a 0.25-fold difference between the cells within the cluster and all remaining cells, and if they were detected in more than 25% of the cells within the cluster. These clusters, which we referred to as subtypes, were then annotated by comparing the cluster markers to previously identified cell type markers reported in the literature for mouse and human datasets. The complete list of markers can be found in Table S1.
When a cluster exhibited enrichment based on the developmental stage, this information was included in the annotation. For instance, the "early RG" cluster was enriched in E25 samples and expressed both common radial glial cell markers shared with other RG clusters in our dataset, as well as early onset genes previously reported in mouse studies (Okamoto *et al*, 2016; Telley *et al*, 2019), such as *HMGA2*, *FLRT3*, and *LRRN1* (Table S1). Therefore, we named this cluster "early RG" based on its age-dependent properties.
To achieve more precise clustering, cycling cells were identified using known markers implemented in the Seurat package, specifically S-phase genes and G2M-phase genes. Clusters enriched in S-phase genes or G2M-phase genes were identified, resulting in the identification of early_RG2 (S), early_RG3 (G2M), late_RG2 (G2M), late_RG3 (S), IPC2 (S), and IPC3 (G2M) clusters (Figure S2B). Subtypes of RG and IPC cell-types were further combined to facilitate data representation.

Differential Gene Expression Analysis
Differential gene expression (DEG) analysis was conducted using “FindMarkers” Seurat function with default parameters.

Pseudotime Analysis
Monocle 2 was employed to construct developmental trajectories based on pseudotime ordering of single cells (Qiu *et al*, 2017; Trapnell *et al*, 2014). A subset of clusters was generated using “SubsetData” Seurat function using the raw counts. Combined progenitor clusters (F_earlyRG, F_midRG, F_lateRG, F_tRG, F_IPC, F_OPC) were selected. Clusteres known to originate from non-cortical sources, including microglia, endothelial and mural cells, were removed prior to pseudotime analysis. The expression matrix and a metadata file that contained above cluster information defined by Seurat were used as input for monocle package (Table S2).
The “differentialGeneTest” function was used to select genes for dimensionality reduction (fullModelFormulaStr = '~Subtype.combined'). Top 1,000 genes were used for cell ordering. The

visualization of the minimum spanning tree on cells was obtained by Monocle2 "plot_complex_cell_trajectory" function. To visualize the ordered cells on Seurat's UMAP plot, the branch information for cells was extracted and added as metadata of the merged Seurat object ("AddMetaData" Seurat function).

Prepocessing of External scRNA-seq Datasets for Comparisons

To compare our ferret scRNA-seq data with that of developing human brain, datasets from Nowakowski *et al*. (2017) and from Bhaduri *et al*. (2021) were used for human samples. All cells included in the analysis and cluster assignments from the provided matrix were mapped to the cell type assignments provided in the metadata of Nowakowski et al. dataset, and the cell type labels were used as provided by the authors without modification. For Bhaduri et al. dataset, GW25 sample was used for clustering by Seurat package, following the same procedures described earlier. In both datasets, low quality cells and clusters annotated based on anatomical regions other than somatosensory cortex were removed. Additionally, cells with less than 200 features were excluded. For Bhaduri et al. dataset, we filtered to cells with at least 200 features, less than 6,500 features and less than 5% mitochondrial genes. This resulted in 25,485 cells from around 180,000 cells in Bhaduri et al. dataset, and in 2,673 cells in Nowakowski et al. dataset.

Regarding the organoid datasets, data from Herring et al. (2022) and Bhaduri et al., (2020) were used, applying the default settings in Seurat. The data drived from organoids at 5-months, 9-months, and 12-months were used from the Herring et al., dataset, while data from organoids at 3-weeks, 5-weeks, 8-weeks, and 10-weeks were used for Bhaduri et al. dataset.

Integration of Human and Ferret scRNA-seq Datasets

In the integration analysis of our ferret dataset with human datasets published by Bhaduri *et al*. (2021) and Nowakowski *et al*. (2017), we used Seurat canonical correlation analysis (Stuart *et al*, 2019). First, a Seurat object was created for each dataset as following the previously described steps. Briefly, each object was individually processed with a normalization and variable features were identified. For human datasets, cells or samples obtained from anatomical regions other than somatosensory cortex were excluded.

The integration anchors between human and ferret Seurat objects were identified using "FindIntegrationAnchors" Seurat function with default settings. The integration was then performed with "IntegrateData" Seurat function. Subsequently, scaling, PCA and UMAP dimensional reduction techniques were applied to visualize the integration results. This allowed the exploration and comparison of cell populations between the ferret and human datasets.

Cluster Correlation Analysis Between Ferret and Human Clusters.

To analyze the correlation between clusters in the ferret and human datasets, we performed a correlation analysis as described in Bhaduri *et al*. (2020), with modifications. Prior to integration, we extracted lists of cluster marker genes obtained using "FindAllMarkers" Seurat function (Table S5A), except for Nowakowski et al dataset, where the marker gene list was provided.

To generate a score reflecting the specificity and enrichment of cluster marker genes, we calculated a "Genescore". The genescore value was obtained by multiplying the average fold change, which represents the gene enrichment, with the percentage of the cells expressing the marker in the cluster (pct.1), divided the percentage of cells from other clusters expressing the marker (pct.2), indicating the specificity. This calculation was applied on the marker genes for a specific human subtype of interest within the space of marker genes for ferret NPC clusters (RG, IPC, OPC and EP).

Genescores were obtained for both ferret and human datasets for all markers shared between human subtype of interest (i.e. oRG) and the ferret NPC subtypes. To assess the correlation and the significance of the correlation for the obtained genescores between ferret and human samples, we utilized the "cor.test" function with the Pearson method. The resulting values and their significance were then represented for NPC populations.
This analysis allowed to examine the correlation between specific NPC subtypes in the ferret and human datasets and assess their similarity and potential conserved characteristics.

Prediction of oRG-like/tRG-like Cells
The cell type marker genes for oRG and tRG cell types were extracted from each human scRNAseq dataset. To precisely predict human oRG-like and tRG-like cells in ferret sample, we removed mature neuron, microglia, and endothelial clusters, as well as clusters assigned as unknown, from individual datasets. After this filtering, we performed an integration of the ferret and human NPC clusters using Seurat package as described in the above section (Stuart *et al*, 2019).
After identification of anchors between human and ferret Seurat objects using "FindIntegrationAnchors", we extracted the information of each pair of anchors, which consisted of one ferret and one human cell. If the human cell in the pair belonged to the oRG (or tRG) cluster in human dataset, we considered the corresponding ferret cell in the same pair as oRG (or tRG)-like cell.

Cluster Score Calculation
To assess the cell type prediction, we calculated a cluster score. Using the marker genes specific to either oRG or tRG cell types, we generated matrices for both datasets using our integrated subsets. Our custom-made R scripts were then applied to these matrices, multiplying the human genescore for each marker gene by the expression values of these genes in all cells in the integrated data. This process resulted in the creation of an "oRG score" or "tRG score" for each cell. The results were visualized using beeswarm and boxplot. Representations to depict the distribution of the scores.

Data Availability
Single-cell RNA-seq data have been deposited in the DDBJ under the number PSUB013536.

Chapter 3

RESULTS

3.1. Onset and Progression of neurogenesis and gliogenesis in ferrets.

3.1.1. Immunohistochemical assessment of the temporal pattern of neurogenesis and gliogenesis.

To elucidate the spatial and temporal dynamics of neurogenesis and gliogenesis in the developing ferret brain, we conducted a series of immunohistochemical analyses on the cerebral cortex at different stages of development. Specifically, we examined embryonic days E25, E32, E36, E40 and postnatal days P5 and P10, which cover these developmental phases (Figure 3.1.1.A-B). We examined the distribution of RG, IPC and oligodendrocyte precursors (OPC), by co-staining for their markers (PAX6, TBR2 and OLIG2 respectively). We also stained for Glial fibrillary acidic protein to investigate the presence of astrocytes and their progenitors (GFAP; Figure 3.1.1.C).

At E32, the PAX6+ RG and TBR2+ IPC were predominantly confined in the VZ and the SVZ, respectively. Neurogenesis had already begun at E25, resulting in an enlargement of TBR2+ IPC-containing SVZ and the expansion of cortical plate (CP) by E32 (Noctor *et al*, 1997). The formation of neuronal layers in the somatosensory cortex was confirmed using two layer-specific markers, CTIP2 (layer V; Arlotta *et al*, 2005) and SATB2 (an upper-layer marker; Szemes *et al*, 2006; Britanova *et al*, 2005). Layer V (CTIP2+) generation was observed during E32 (McConnell, 1988; Poluch & Juliano, 2015). Subsequently, SATB2+ neurons appeared in both deeper and upper sides of the CTIP2+ layer, indicating the production and migration of SATB2+ upper-layer neurons by E36 (Figure 3.1.1.B).

GFAP+ RG with the gliogenic potential appeared at E40, while GFAP+ mature astrocytes with a typical astrogenic morphology emerged outside of the germinal layers at a later stage, around P5 and onwards (Figure 3.1.1.C). Over the course of postnatal development, a progressive increase in OLIG2+ oligodendrocytes and their precursors (OPC) were observed (Figure 3.1.1.A).

Apart from the VZ, PAX6+ progenitors started dispersing outside of VZ throughout the cortex around E32 (Figure 3.1.1.A), subsequently giving rise to OSVZ by E36 (Hansen et al., 2010; Fietz et al., 2010; Reillo et al., 2011). The parietal OSVZ attained its peak expansion around birth (Figure 3.1.1.A), and gradually regressed by P10.

Prior research has established that oRG cells residing in the OSVZ are multipotent and contribute to upper-layer neurogenesis. Recent reports have also unveiled that cortical OPCs are derived not only from RG in the ventral telencephalon, but also from RG in the dorsal cortex in both mice (Zheng *et al*, 2018) and humans (Rash *et al*, 2019; Huang *et al*, 2020), challenging the earlier assumption that OPCs were primarily originate ventrally. To assess whether some OPCs in ferrets also from the dorsal region, we labeled RG in the dorsal cortex of ferrets at E30 via in utero electroporation of an mCherry-expressing vector (Figure 3.1.1.D; see also Methods). By P10, we observed mCherry+ OPC (OLIG2+ PAX6+) in both VZ and OSVZ (Figure 3.1.1.D-E). This result revealed the production of cortical OPCs by dorsal RG in ferrets, aligning with the findings in mice and humans.

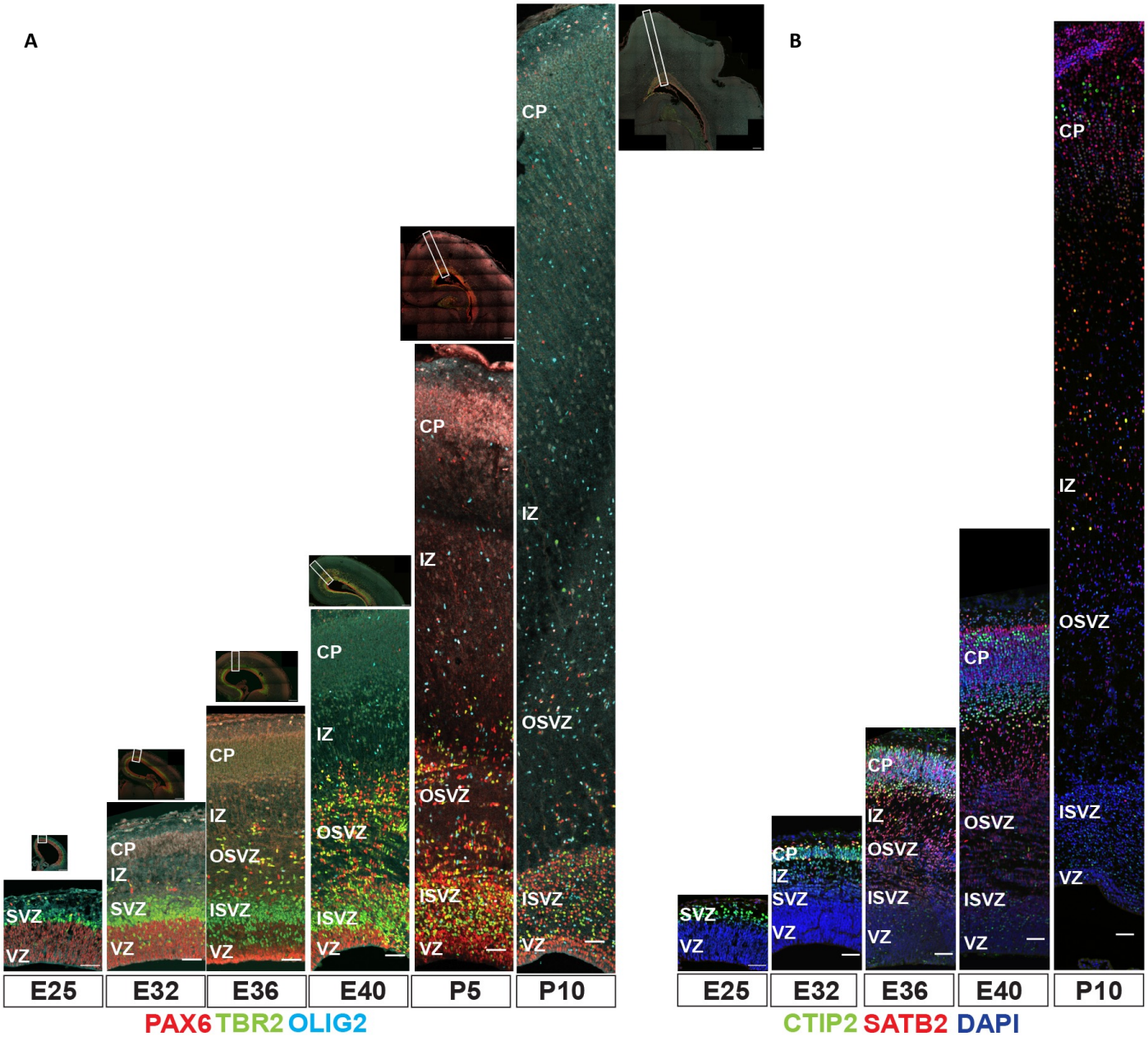
A
B
CP
IZ
OSVZ
ISVZ
SVZ
VZ
E25
E32
E36
E40
P5
P10
PAX6 TBR2 OLIG2
CTIP2 SATB2 DAPI

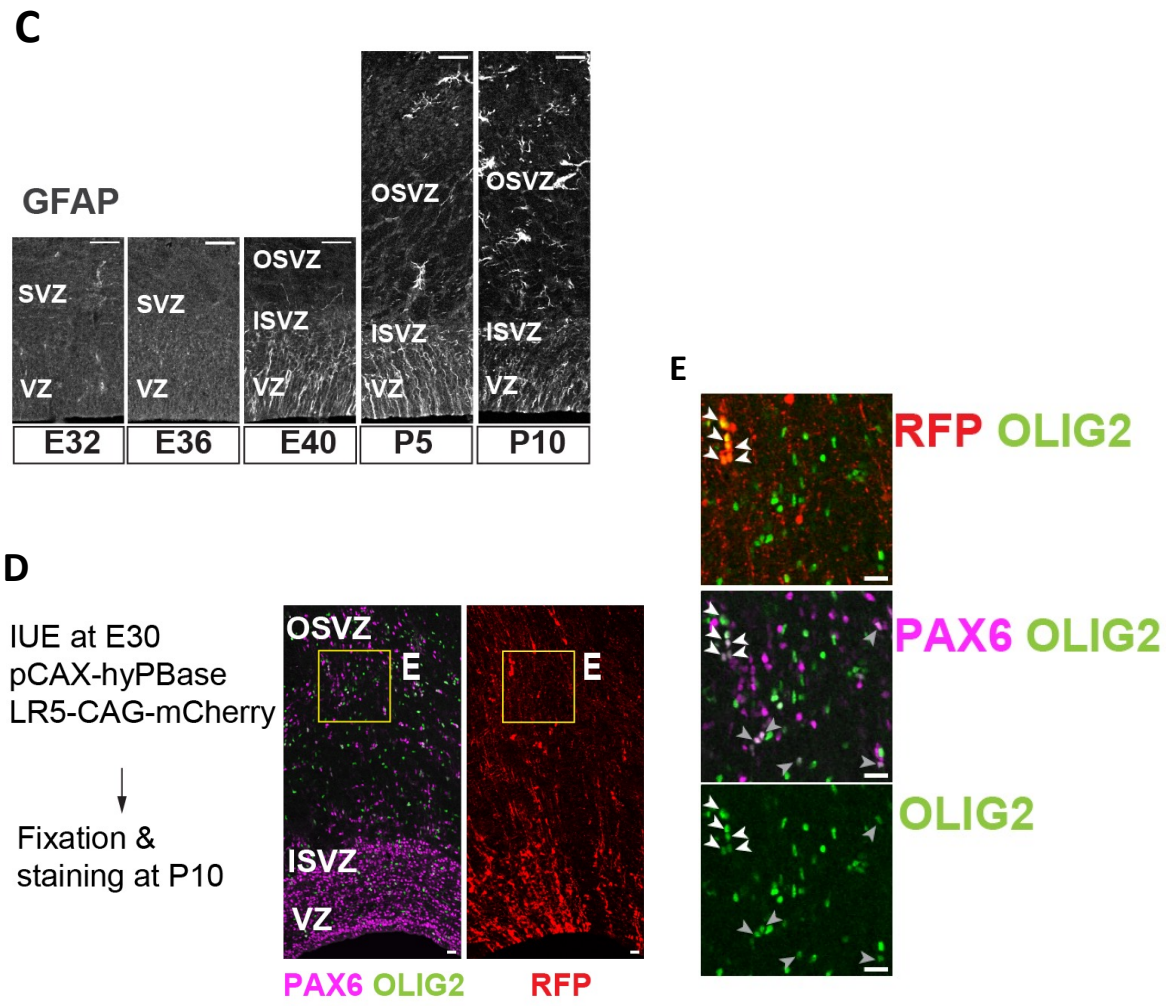

Figure 3.1.1. The cellular composition of cerebral cortex during ferret brain development. **A.** Coronal section of the dorsal cortices immunostained for RG (PAX6, red), IPC (TBR2, green), and OPC (OLIG2, cyan) from early to late neurogenesis at E25, E32, E36, E40, P5, and P10. Scale bars = 100 µm. The position of the image strip at each stage is shown in the corresponding dorsal hemisphere image above the strip. The approximative boundaries of dorsal cortex area used for single-cell RNA sequencing are highlighted with dotty line segments in the dorsal cortex hemisphere above each strip. **B.** Immunostaining for CTIP2 (green) and SATB2 (red) at the same developmental stages as in (**A**), showing the onset of DL- (E25 or earlier) and UL-neurogenesis (E32–E34). Scale bars = 100 µm. **C.** Immunostaining for GFAP, a marker showing gliogenic cells and astrocytes, in cortical germinal layers at E32, E36, E40, P5, and P10. Gliogenic progenitors emerge around E40, while mature astrocytes with a typical astrocytic morphology appear later at approximately P10 onward in the outside of the germinal layers (Reillo & Borrell, 2012). **D, E.** Immunostaining of cortical sections for PAX6 (cyan), RFP (red) and OLIG2 (green). mCherry labeling of the dorsal cortex at E30 showing that a population of OLIG2^{+} oligodendrocyte precursors are generated in the cerebral cortex by P10 as reported for both mice and humans (Zheng *et al*, 2018; Rash *et al*, 2019; Huang *et al*, 2020; Kessaris *et al*, 2006). **E.** Arrowheads in the cropped images of the left panels indicate cells that co-express mCherry, PAX6, and OLIG2 in the OSVZ. Scale bars = 20 µm.

3.1.2. Comparison of progression of temporal pattern-genes in VZ and SVZ by *in situ* hybridization.

Changes in the temporal identity of self-renewing neural progenitor cells along the progression of brain development stand for a key determinant of the neuronal diversity in cortical layers, and influence the progression of sequential developmental events from deep-layer neurogenesis to upper-layer neurogenesis, followed by the gliogenesis from NPCs (Figure 3.1.2.A). These transiently expressed genes in NPCs may influence over the fate of their lineage. While this concept has been explored to a limited extent with certain temporal markers, such as *Zbtb20* - a late-onset gene renowned for its crucial role in upper-layer neurogenesis and the gliogenic switch (Tonchev *et al*, 2016; Nagao *et al*, 2016)- the assessment of this idea remains incomplete.

The temporal changes occurring in progenitor cells play an essential role in understanding how the positioning and diversity of neurons are established throughout mammalian brain development.

In ferrets, these events are accompanied by the formation of OSVZ and its expansion (Figure 3.1.2.B). Matsuzaki laboratory's previous study revealed a set of genes that represent the temporal identity of progenitor cells isolated from mouse cortex that develops from single germinal layer (Okamoto et al., 2016). Nevertheless, in complex brains that are formed from multiple germinal layers, it remains unknown whether and how the clock in different self-renewing progenitors at the complex brain-specific germinal layer proceed during development. To elucidate this phenomenon, we resort to two major approaches utilizing ferrets as a model system for Gyrencephalic brains. First, we analyze the temporal and spatial patterns of the mouse clock markers in the ferret brain using *in situ* hybridization.

During mouse cortical brain development, *Dkc1* and *Gja1* are early-onset genes expressed strongly at E12.5 (proliferative stage) and eventually reduced at E14.5 (neurogenic stage) and E16.5 (late-neurogenic stage). Conversely, the expression of *Apoe* intensifies starting from E16.5 (Figure 3.1.2.C). Here, the expression of *PAX6*, was used as a self-renewing progenitor cell marker, and the mentioned genes stands as representatives for temporal pattern-related markers among over twenty genes tested, shown across the relevant stages on fixed ferret cortex (Figure 3.1.2.E). As expected, the ferret cortex mirrors a comparable temporal pattern in the VZ to that observed in mice, except for *GJA1*, whose expression continues throughout later stages and exhibits a delayed presence in the SVZ (Figure 3.1.2.D-E). Our observations revealed that early-onset genes did not exhibit subsequent expression within the SVZ, indicating that the emerging OSVZ do not express these markers.

Furthermore, the progression of temporal patterning aligns similarly between the VZ and the ISVZ for late-onset genes, as contrasted with the OSVZ. These findings suggest, that during the neurogenic period in the ferret cortex, the temporal expression pattern similarly progresses between VZ and ISVZ, but not in with the OSVZ. The divergence in the OSVZ suggest different regulations of gene expression, and specie-specific variations in neurogenic processes.

A

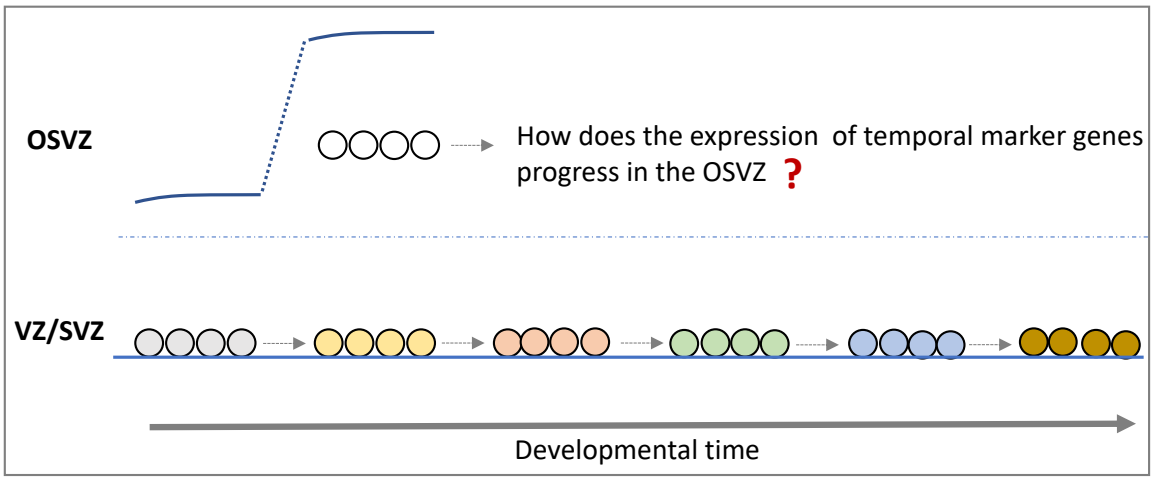

B

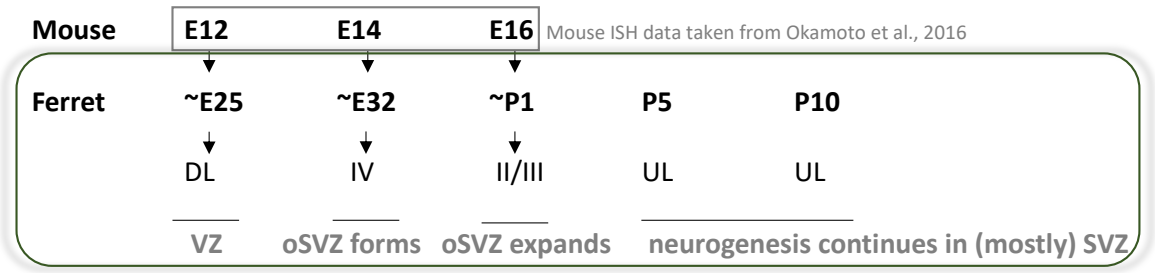

C **Summary for temporal gene expression trends in the mouse cortex (Okamoto et al., 2016)**

Temporal genes	E11-high RG	E11-high RG+IP	E14-high RG	E14-high RG+IP	E16-high RG	E16-high RG+IP
Dmrta1		o				
Dkc1	o					
Gja1	o					
Aldoc				o		
Bai3				o		
Tnc						o
Apoe						o

D **Summary for *In Situ* Hybridization data on developing ferret brain**

Temporal genes	E32	E36	P1	P5	P10	Germinal layer
Dmrta1	o	-	-	-	-	VZ
Dkc1	**o**	**o**	o*	-	-	VZ
Gja1	o	o	o	**o**	**o**	VZ/ISVZ
Aldoc	o	**o***	**o**	**o**	o	VZ/ISVZ/OSVZ
Bai3	**o**	**o**	**o**	**o**	o	VZ/ISVZ
Tnc	**o**	**o**	**o**	**o**	**o**	VZ/ISVZ/OSVZ
Apoe	-	o	**o***	**o**	**o**	VZ/ISVZ

****transition stage of gene expression pattern.***

E

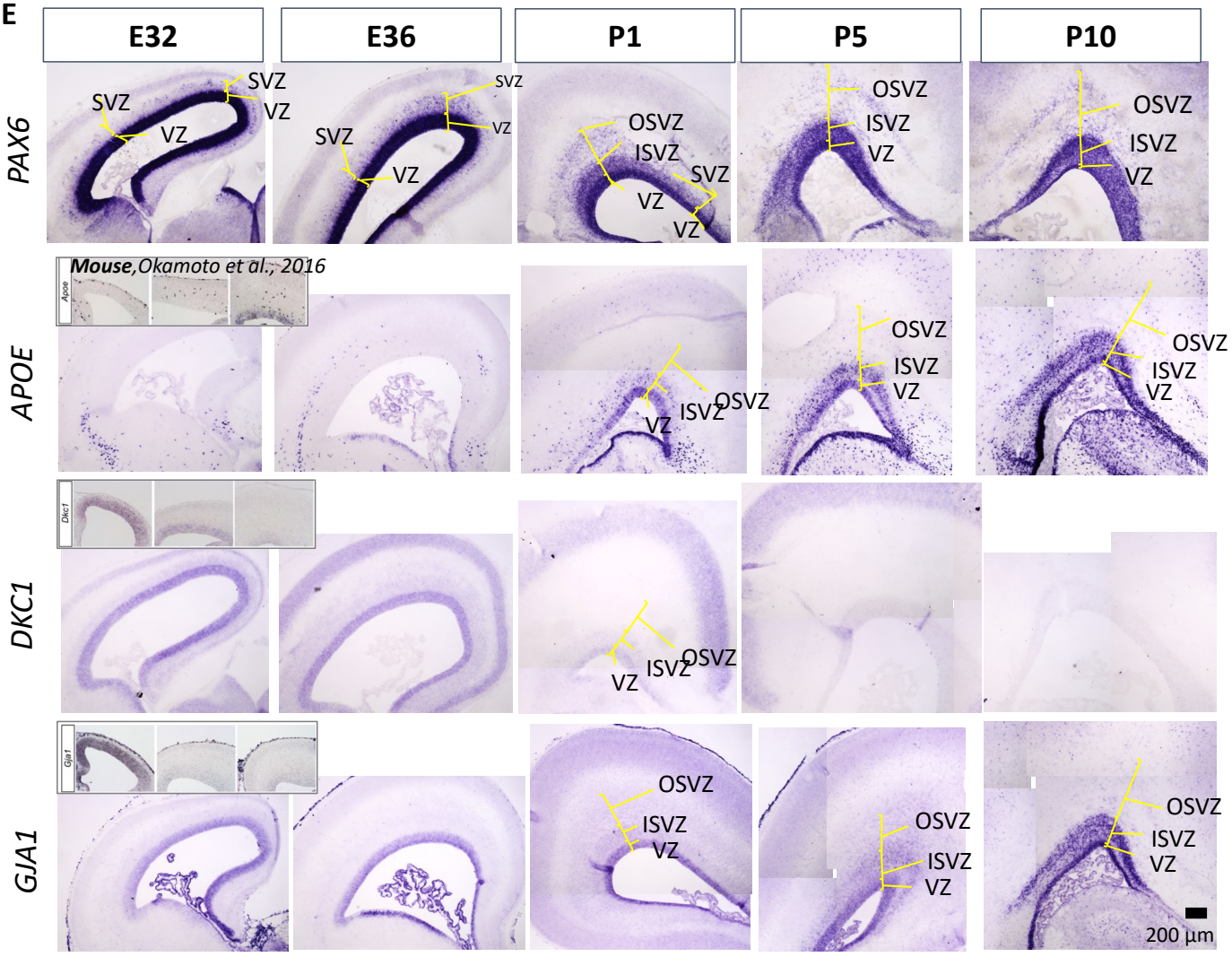

Figure 3.1.2. Comparison of the expression pattern of temporal markers between VZ and OSVZ.
A. Illustration depicting the progression of temporal pattern genes in the VZ, ISVZ, and OSVZ regions of ferret brain development. **B.** Comparative diagram illustrating the developmental milestones in the cerebral cortex of mice and ferrets. **C.** Tabular presentation summarizing the temporal gene expression patterns in the mouse cortex, derived from Okamoto et al., 2016. **D.** Tabular representation summarizing the temporal gene expression trends in the ferret cortex, as determined through in situ hybridizations (as depicted in E). **E.** In situ hybridization analysis of ferret brain tissue, targeting *PAX6*, *APOE*, *DKC1*, and *GJA1*, across different developmental stages.

3.2. Single-cell transcriptomics revealed cellular diversity in developing ferret brains.

To achieve a more detailed assessment of the temporal pattern progression and to reveal cellular diversity, we next focused on conducting single-cell transcriptional profiling of cortical cells in ferrets.

3.2.1. Single-cell RNA-sequencing recapitulated subtypes of cortical cells in ferrets.

While prior transcriptome studies have explored the ferret cortex, a notable gap exists in our knowledge of the ferret genome, particularly concerning the 3'-untranslated regions of genes (Johnson et al, 2018; de Juan Romero et al, 2015). This limitation has posed challenges for achieving high-resolution single-cell transcriptome analyses, which are crucial for accurate comparisons with human datasets. To overcome this, we first undertook an effort to enhance the annotations of ferret genomic DNA using Chromium genomic droplet sequencing. The new gene models were constructed in collaboration with Kuraku Laboratory from RIKEN BDR (Bilgic et al., 2023).

To decipher the temporal trajectories of cell types during ferret brain development, we conducted single-cell RNA sequencing of the ferret dorsal cortex at six developmental time points that cover proliferative, neurogenic and gliogenic phases of neural progenitors. To enrich progenitor subtypes, we employed two approaches: (1) FACS-based sorting of the neural progenitor cell fraction marked by an AzamiGreen (AG)-driven HES5 promoter (Ohtsuka et al, 2006), and (2) isolation of cells from VZ, SVZ and intermediate zone (IZ) of cerebral cortices, while excluding the cortical plate (CP) enriched with differentiated neurons (Figure 3.2.1.A). By merging these two cell populations across all sampling stages, we performed unsupervised clustering. The resultant clustering of cells was visualized in the Uniform Manifold Approximation and Projection (UMAP) space (preprint: McInnes et al, 2018; Stuart et al, 2019). Our analysis unveiled 26 transcriptionally distinct clusters among 30,234 ferret cortical cells spanning the course of corticogenesis (Figure 3.2.1.A). Notably, each cell cluster was annotated based on its unique gene expression patterns and categorized into ten major cell types: early, mid, and late RG, IPC, OPC, ependymal cells (EP), excitatory cortical neurons (deep layer and upper layer), inhibitory neurons, microglia, endothelial cells, mural cells and a cluster of cells with currently unknown identities (Figure 3.2.1.D).

RG clusters (expressing *VIM*, *PAX6*, and *HES5*), IPC (expressing *EOMES*, *NEUROD4*, and *HES6*), and neuronal clusters (expressing *STMN2* and *NEUROD6*) were aligned in the UMAP plot according to the neuronal differentiation process (Figure 3.2.1.B). Further refinement of RG

cells led to their classification into three subclusters (early, mid, and late), determined by their collection stages and the expression of temporally regulated RG markers previously reported as temporal indicators (Okamoto et al, 2016; Telley *et al*, 2019). The "early RG" clusters predominantly comprised cells from E25, whereas the "mid RG" clusters were primarily composed of E34 cells (Figure 3.2.1.C). *HMGA2, LDHA,* and *LIX1* for early RG, and *PTN, ALDOC,* and *FABP7* for late RG were used as temporal markers (Figure 3.2.1.D-E). The "early RG" clusters comprised E25 cells; "mid RG" clusters, mostly of E34 cells, and "late RG" groups, with cells from E34 and later stages. Therefore, RG clusters were distinguished according to their sequential transcriptional profiles rather than a sample batch. These changes in the transcriptional profiles of RG along the temporal and differentiation axes were consistent with the *in vivo* development.

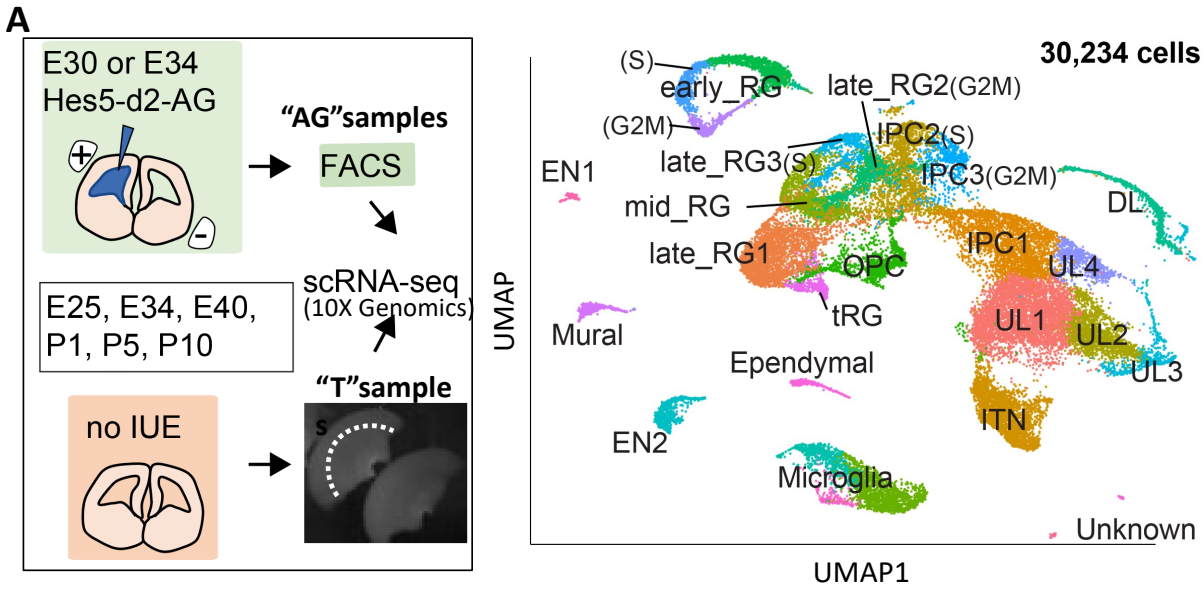

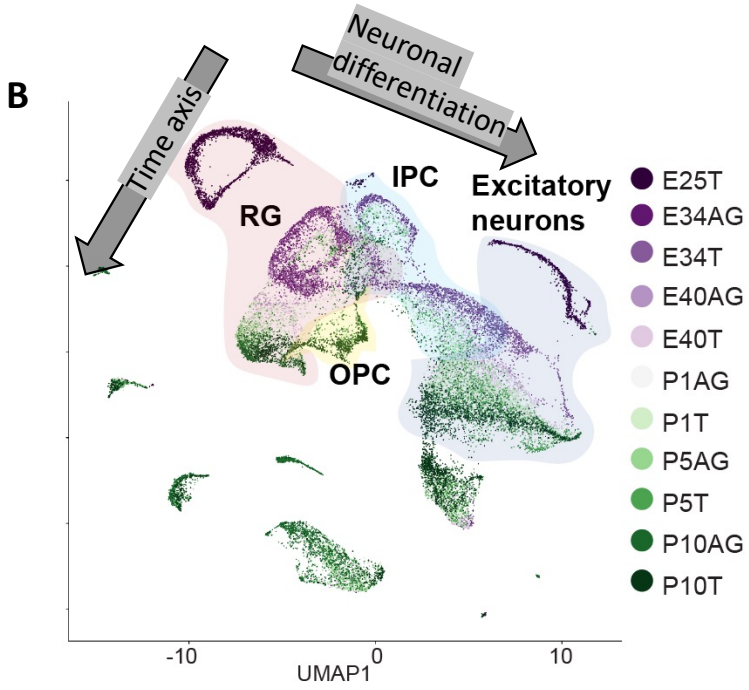

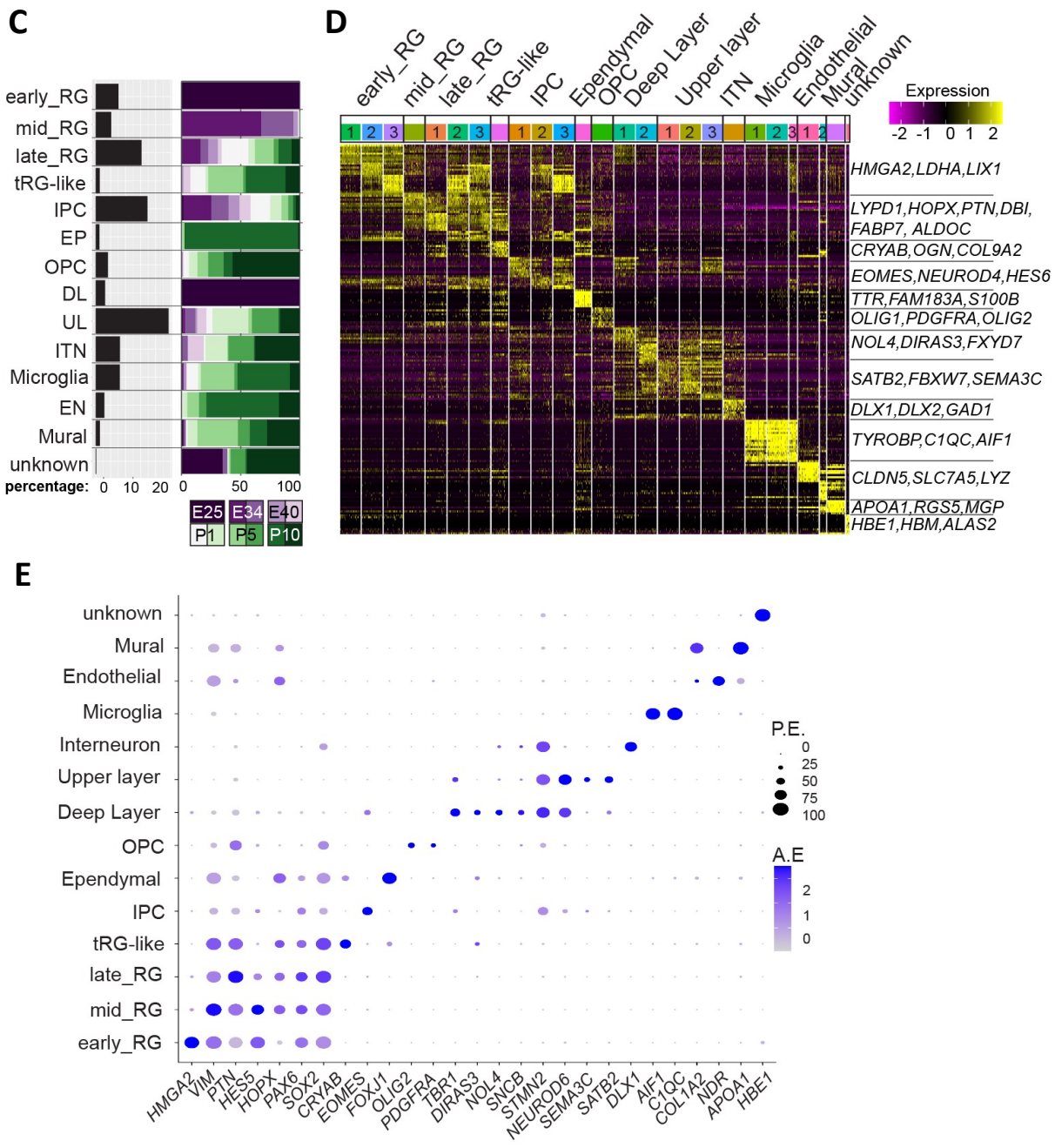

Figure 3.2.1. Single-cell RNA-sequencing recapitulated subtypes of cortical cells in ferrets. **A.** Schematic representing the experimental design and time points used to build the transcriptome atlas of developing somatosensory cortex of ferrets (left). Single cells were isolated using 10X Chromium. UMAP visualization shows cells colored by Seurat clusters and annotated by cell types (right). **B.** UMAP visualization showing cells colored by sample. Radial Glia (RG), intermediate progenitors (IPC), excitatory neurons and oligodendrocyte precursors (OPC) are highlighted. Cells are distributed by a time axis and a neuronal differentiation axis. **C.** Percentage of each cell type in the merged dataset (right) and percentage of collection stages in each cell type (left). **D.** Heatmap showing expression profiles of cluster marker genes based on log fold-change values. Cells were

grouped by Seurat clustering (transverse). Cell types were assigned according to the expression of marker and differentially expressed genes in each cluster. Early RG was defined by the expression of *HMGA2, LDHA,* and *LIX1*; and late RG, by *PTN, ALDOC,* and *FABP7*. Color bar matches the Seurat clusters in A. The ten most enriched representative genes in each cluster are shown. **E.** Dotplot showing average expression and percentage of expression of representative marker genes for individual cell types in the merged dataset. P.E., percentage of expressing cells per cell type; A.E., average expression per cell type.

3.2.2. Ventricular RG (vRG) of VZ and outer RG (oRG) of SVZ were transcriptionally indistinguishable throughout ferret brain development.

During ferret brain development, oRG and vRG cells did not segregate into distinct clusters based on their transcriptional profiles (Figure 3.2.1.A, D). This indistinguishability persisted throughout various stages of the development. The lack of separation within the clustering suggests a similarity in the gene expression patterns of these two cell types. In contrast, human and primate studies consistently display distinct transcriptomic profiles between oRG and vRG cells.

To validate these observations, we pursued IHC and *in situ* hybridization (ISH) analyses targeting the markers typically attributed to human oRG, such as *CLU*, *HOPX*, *MOXD1* (Pollen *et al*, 2015). These markers were not exclusive to ferret oRG but were expressed across both VZ/ISVZ and OSVZ, as similarly reported in previous reports (Figure 3.2.2.A-B; Kawaue *et al*, 2019; Johnson *et al*, 2018).

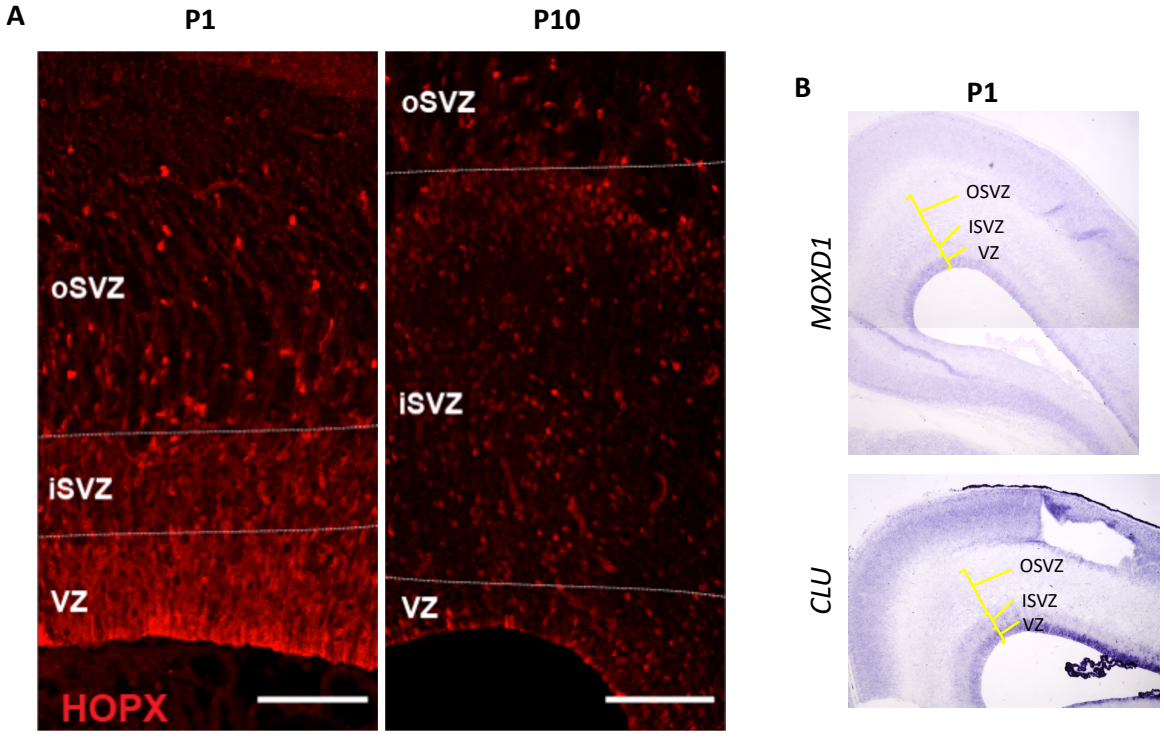

Figure 3.2.2. Human-specific oRG markers were not specific to OSVZ in ferrets.
A. Immunohistochemistry for HOPX on the germinal layers of the ferret cortex at P1 and P10. **B.** In situ hybridization against MOXD1 and CLU on ferret cortex at P1.

3.2.3. Unveiling a tRG-like cluster through scRNA-seq analysis.

While the separation between oRG cells and vRG cells was not evident through unbiased clustering in ferrets as mentioned earlier, we noticed a distinct cluster comprising 409 *PAX6*-expressing RG subtypes emerged, of which 69% expressed *CRYAB* (Figure 3.2.1-A; 3.2.3A-B). *CRYAB*, known for encoding a molecular chaperone (Yamamoto *et al*, 2014), serves as a unique marker for human tRG (Nowakowski et al., 2016; Pollen et al., 2015). The expression of *CRYAB* was confirmed *in vivo* using ISH and was restricted to the VZ in ferrets (Figure 3.2.3.C). Consequently, we classified them as tRG-like cells in ferrets, and confirm their cellular features by *in vivo* assessments described later.

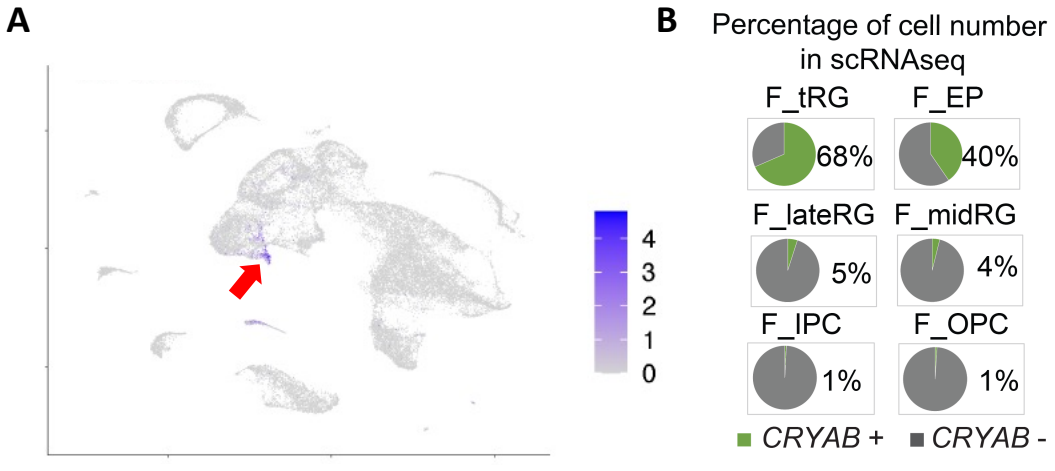

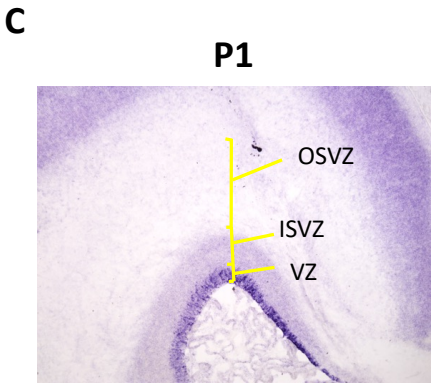

Figure 3.2.3. The emergence of tRG in developing ferret cortex.
A. The expression pattern of *CRYAB*, a marker for tRG, only described in humans and other primates, on UMAP. **B.** Pie charts showing the percentage of *CRYAB* expression in the ferret clusters of the merged transcriptome dataset of all stages. Cells were counted as positive if the count of unique molecular identifier (UMI) for *CRYAB* was > 1 using Seurat "WhichCells" function (slot = "counts"). **C.** In situ hybridization of *CRYAB* on cortical sections at P1.

3.3. Comparison of developmental transcriptomic profiles between ferrets and humans.

3.3.1. Integration reveals shared developmental trajectories in ferret and human single-cell transcriptomes.

Ferrets and humans represent characteristics of gyrencephalic mammals, although they reside in distinct phylogenetic branches. Notably, ferrets have emerged as a valuable model organism, offering a unique avenue to bridge the gap in our understanding of complex brain development. A comparison of radial glia (RG) subtypes and their nuanced temporal patterns of birth, transitions, and differentiation is hence particularly crucial due to their utilization as an

alternative to human studies. Moreover, such a comparative approach holds immense potential in unraveling species-specific developmental processes that contribute to the formation of complex brains. In this study, by takin advantage of the power of single-cell transcriptome analysis, we inaugurated an attempt to compare our comprehensive ferret dataset with a well-established human counterpart (Nowakowski et al., 2017). The integration of these datasets was performed using the Seurat package, which relies on the identification and pairing of cells exhibiting highly similar transcriptional states. This alignment was achieved through the mutual nearest neighbors (MNNs) following Canonical Correlation Analysis (CCA) of the datasets (Stuart *et al*, 2019; Methods). This computation resulted in clustering of similar cell types together, including RG, IPC, OPC, neurons, mural cells, endothelial cells, and microglial cells, across both datasets (Figure.3.3.1.A).

The integration also highlighted the similarities between developmental stages of ferret and human brains as shown on the UMAP plot (Figure.3.3.1.B). Cells from ferret E25 shared proximity with their human GW8 counterparts, while ferret E34 clustered alongside human GW11-14 cells. Likewise, ferret E40-P1 cells converged with human GW15-16 cells, and the final alignment paired ferret P5-P10 cells with human GW17-22 cells. This integration emphasizes the shared developmental trajectories between the two species. Furthermore, consistently with our in vivo observations above, the subtypes of gliogenic RG cells, nested within the "late_RG" group, and OPCs, were first observed at E40 in the ferret dataset and at GW15 in the human dataset (red arrows in Figure 3.3.1.B).

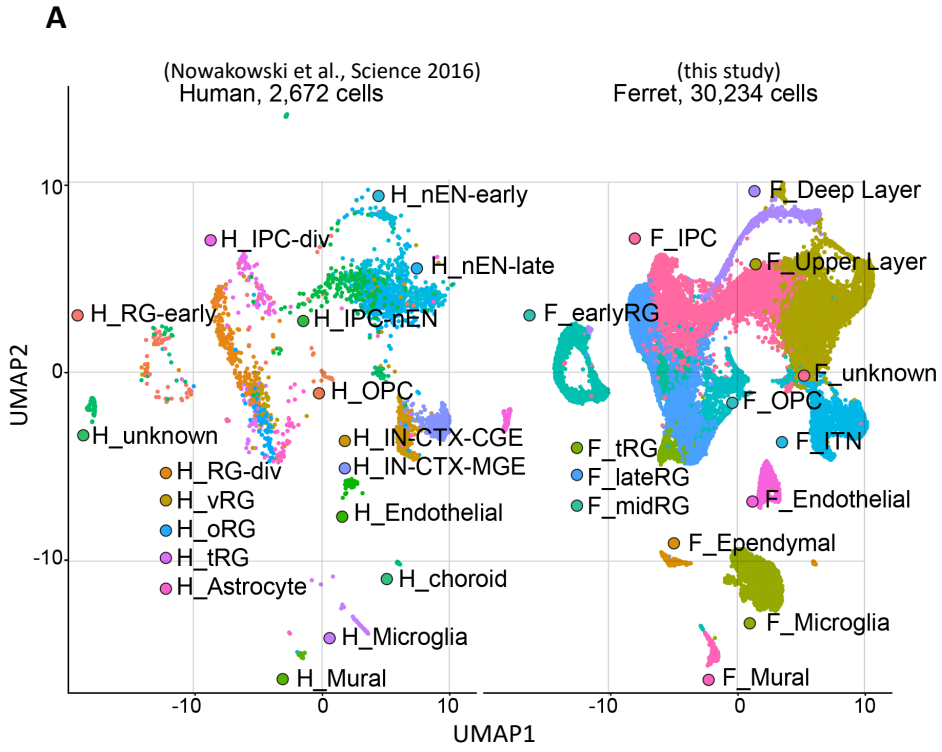

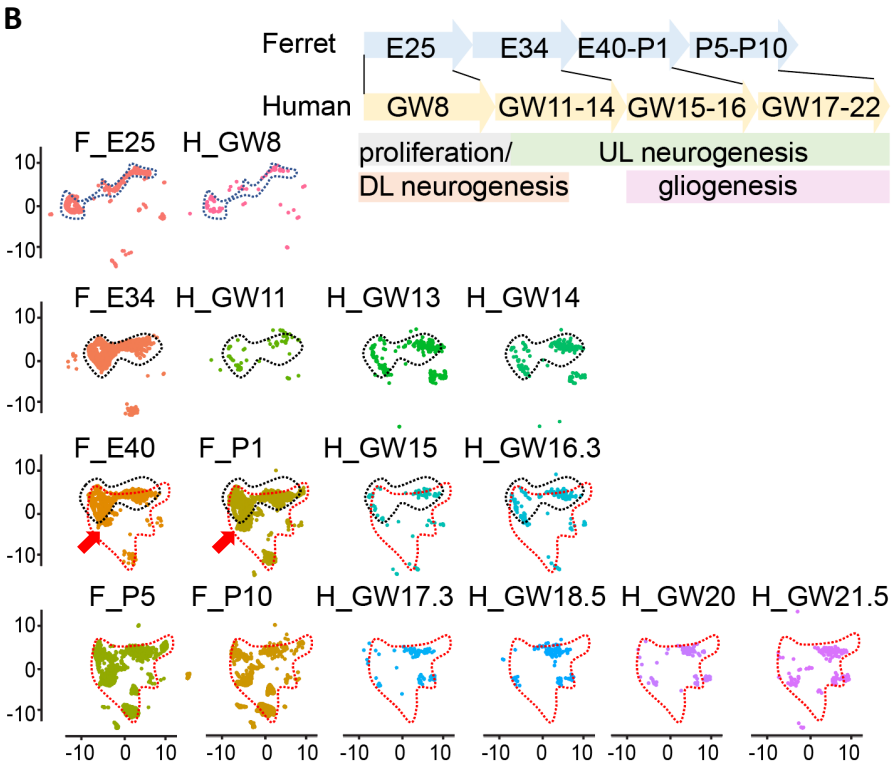

Figure 3.3.1. Shared developmental trajectories in ferret and human single-cell transcriptomes.
A. UMAP visualization of integrated human (n = 2,672; left) and ferret (n=30,234; right) single-cell datasets colored according to the different clusters. The names of clusters from human and ferret cells begin with "H" and "F," respectively. **B.** Homologous temporal pattern of transcriptomic characters of progenitors and their progenies between ferrets and humans. Corresponding neurogenic stages between ferrets and humans can be assigned by cell distribution at homologous positions in UMAP plots. Gliogenic RG cells (a subtype of the "late_RG" group and OPC) were first distinguished transcriptionally at ferret E40 and at human GW14, as pointed out by red arrows.

3.3.2. The radial-glia subtypes in ferrets correlate with their human counterparts.

To further reveal shared and divergent RG subtypes in an unbiased manner, we sought to quantify the features of RG subtypes in both species. Employing the marker-gene score parameter, we evaluated the correlation between RG subtypes in ferrets and humans. This analysis confirmed that the early and late RG clusters exhibited significant similarity across species (Figure.3.3.2.A). Furthermore, transcriptome profiles between ferret tRG-like cells and human tRG were significantly correlated. Notably, key markers such as *CRYAB*, *EGR1* and *CYR61*, indicated the close alignment of tRG-like clusters in both species (Figure.3.3.2.B).

To assess the cell-cell similarity further, we introduced a "cluster score" for each individual cell. This score is determined by a linear combination of a cell's marker gene expression levels, with each contribution weighted by the genescore of the corresponding human cluster. When we computed the cluster score for ferret tRG cells using genescores from the human tRG cluster, the resulting score surpassed that of any other cluster in both datasets (Figure.3.3.2.C). These findings affirm, based on transcriptomic data, the proximity between the ferret tRG cluster and its human counterpart.

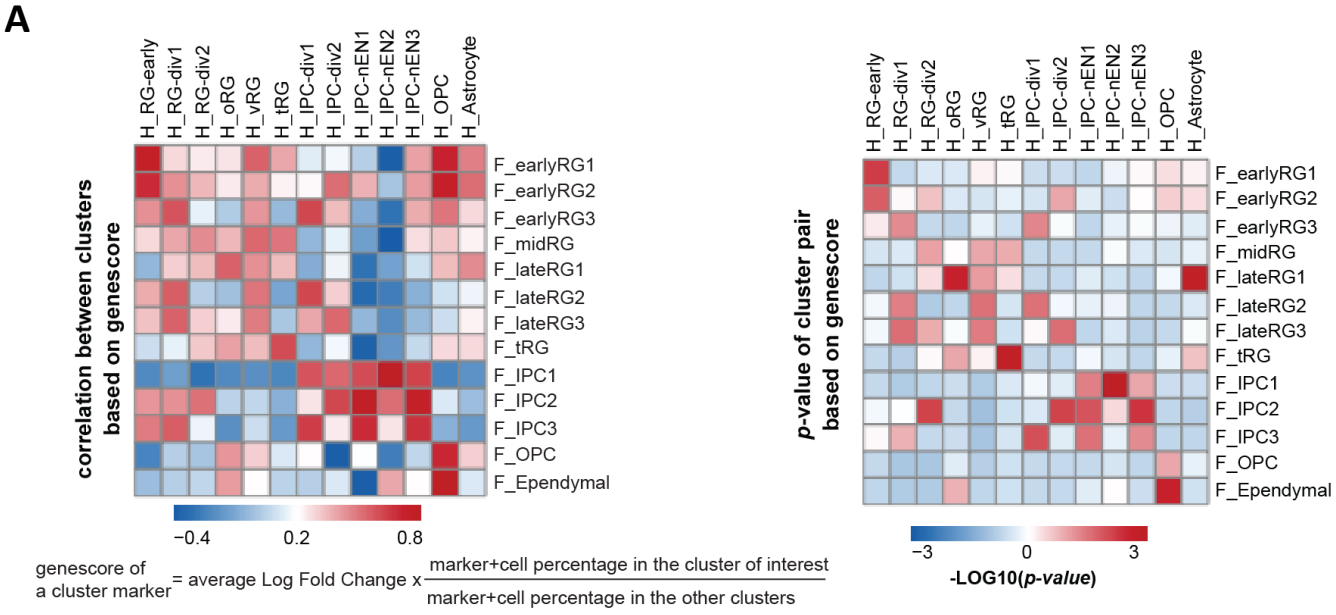

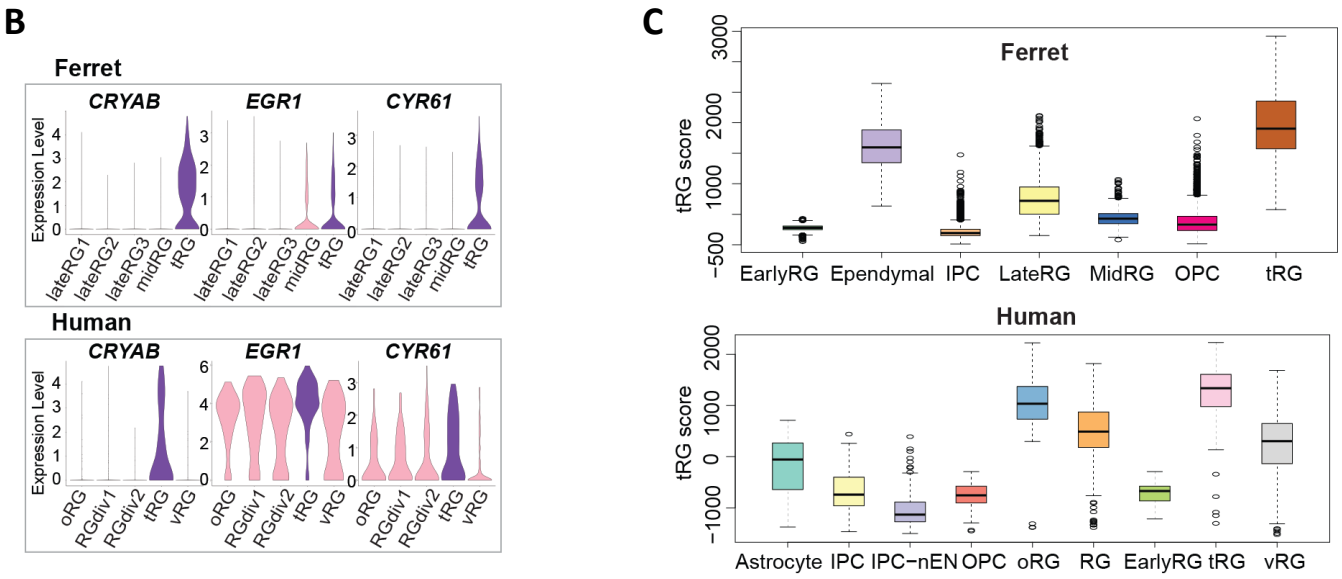

Figure. 3.3.2. The radial-glia subtypes in ferrets correlate with their human counterparts. **A.** Correlation coefficient (left) and significance (right) between indicated clusters of ferrets and humans, calculated by marker gene scores (see Methods for details). **B.** Normalized expression levels of the indicated genes in humans and ferrets from each progenitor cluster. **C.** tRG scores of the indicated clusters are presented as box and whisker plots for humans and ferrets. As for the definition of cluster scores, see the text and Methods. These represent the range without outliers (lines) and upper and lower quartiles with the median (box). Outliers are represented as points outside the box. Outliers are 1.5-fold larger or smaller than interquartile range from the third or first quartile, respectively.

3.3.3. Prediction of ferret oRG-like and tRG-like cells through cluster scores.

As previously mentioned, in the ferret dataset , a distinct cluster corresponding to oRG was lacking. To address this, we aimed to identify oRG-like cells within the ferret dataset by using human oRG cells as reference. Through the integration approach, we attempted to assign ferret cells in close proximity to the human oRG cells as oRG-like cells. First, we have used publicly available transcriptome dataset of NPCs of GW28 human brains (Figure.3.3.3.A; Bhaduri *et al*, 2021). Using only NPC clusters in both species, we have integrated ferret and human datasets (Figure.3.3.3.B).

We then assigned ferret oRG through the integration of two datasets utilizing the MNN technique following CCA alignment. As a result of this approach, oRG-like cells were successfully assigned, primarily situated in proximity to the human oRG cluster (Figure.3.3.3.C). To quantify the degree of resemblance to human oRG, we employed the computation of an oRG score for each ferret oRG-like cell, analogous to the procedure performed for tRG cells earlier. The allocated oRG-like cells exhibited significantly elevated oRG cluster scores in comparison to the entirety of other NPCs (Figure.3.3.3.C).

Furthermore, we identified genes that were highly expressed in oRG-like cells by comparing the gene expression profiles of oRG-like cells with those of other NPCs in the ferret dataset. Similar to the findings in the human dataset (Bhaduri et al., 2021), the expression of *HOPX*, *CLU*, and CRYM genes was notably higher in oRG-like cells compared to other NPCs in the ferret dataset (Figure.3.3.3.D). However, certain human oRG markers, like HOPX and CLU, were also expressed by vRG and tRG cells in ferrets as described earlier. This suggests that, at the transcriptome level, oRG cells requires an assessment of the overall transcriptome similarity or considering a combination of several markers, rather than relying solely on a small set of marker genes.

Taken altogether, despite a significant difference in developmental timescale between humans and ferrets, there was a conserved diversity and temporal trajectory in neural progenitor cells (NPC). The similarities in NPC characteristics between these species suggest fundamental shared mechanisms in cortical development among Gyrencephalic mammals. Furthermore, we identified a tRG-like cluster in ferrets, which shared similar transcriptional profile with their human counterparts, suggesting the presence of this cell type with a yet unknown function in Gyrencephalic mammals.

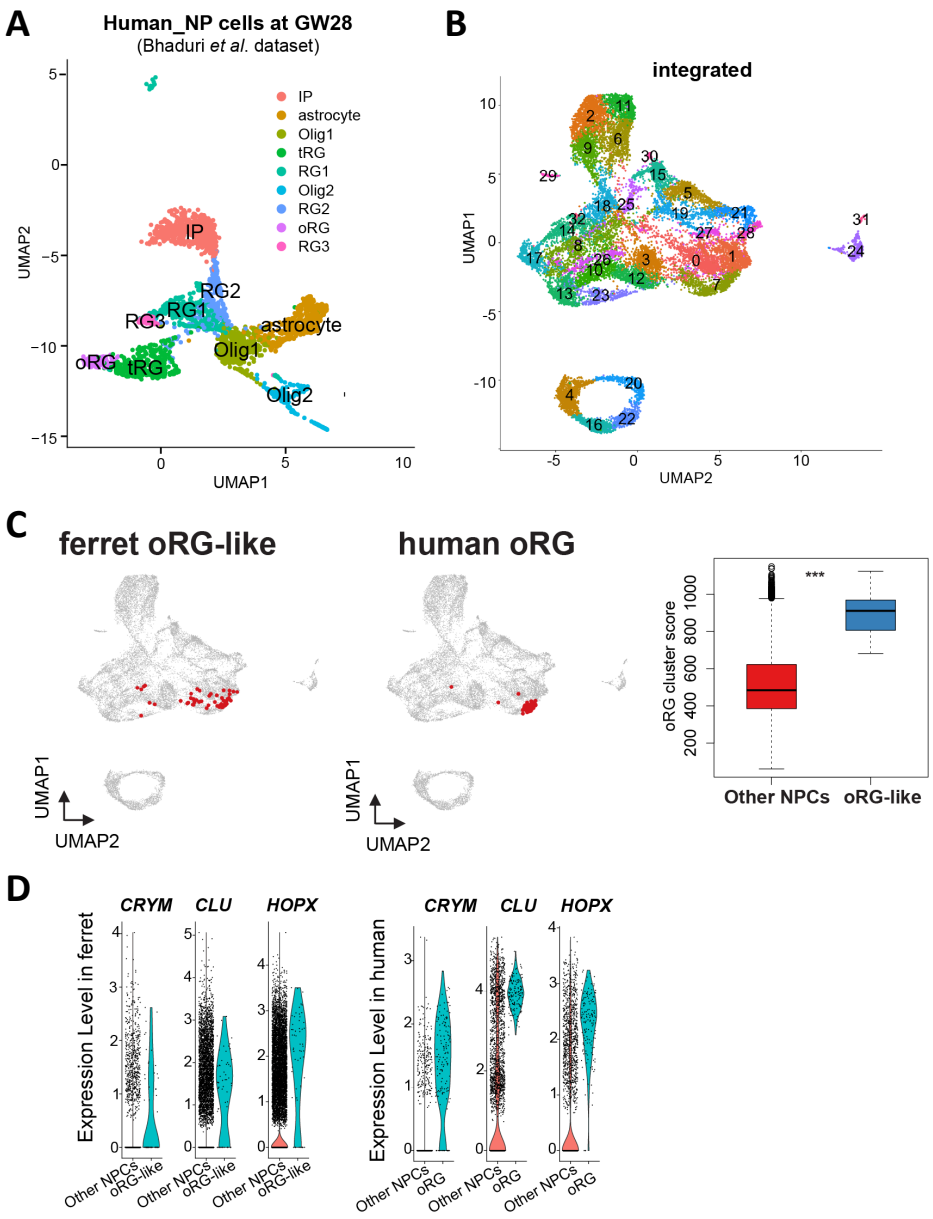

Figure 3.3.3. Prediction of ferret oRG-like cells through cluster scores.
A. UMAP visualization of human brain cells at GW25 (and removing neurons and other cell types). Cells are colored by cell type and identified by marker genes (data from Bhaduri et al, 2021). **B.** UMAP visualization of integrated ferret and human datasets colored and numbered by different clusters. **C.** Identification of oRG-like cells in ferret (left) and oRG cells in human (middle) by cluster score analysis (see the text and Methods for details). All cells are highlighted as red dots. oRG scores for oRG-like cells and other NPCs in ferrets are shown (right). The result indicates that oRG-like cells share more transcriptomic features than other NPCs, whereas ordinary clustering among ferret NPCs failed to distinguish oRG-like cells from the rest. Box and whisker plots indicate ranges (lines) and upper and lower quartiles with the median (box). **D.** The expression levels of *CRYM*, *CLU*, and *HOPX* in oRG-like cells and other NPCs in ferrets (left) and humans (right).

3.4. Exploring tRG as a shared progenitor cell type in Gyrencephalic mammals.

3.4.1. *In vivo* identification of tRG through distinct morphology and marker protein expression in developing ferret brain.

A molecular distinction of oRG in our analyses both *in vivo* and *in silico* was not apparent. On the other hand, we identified a tRG-like cluster in ferret transcriptomes, which led us to explore properties of these cells as their functions in human brain remains unknown. To explore the emergence of such RG cells in developing ferret cortical tissues and their characteristics, we performed sparse labeling of NPC by electroporating P0 pups with an expression vector for EGFP. Remarkably, we observed a distinct cell population displaying key characteristics reminiscent of human tRG (Figure.3.4.1.A; Nowakowski et al., 2016). These features included the expression of *CRYAB*, accompanied by an apical endfoot and truncated basal fiber, localized within VZ during late neurogenesis.

In humans, tRG cells become noticeable and express *CRYAB* during late neurogenic and early gliogenic stages (Nowakowski et al., 2016). Likewise, in ferrets, tRG-like cells exhibited a similar pattern, with the emergence of *CRYAB* expression occurring just prior to birth, specifically during the late neurogenic and early gliogenic stages (Figure.3.4.1.B). This expression became primarily confined to tRG-shaped cells within the VZ and SVZ. The population of these cells increased in number by P10. These observations align with our transcriptome data, indicating a rise in the tRG-like cell population during postnatal development (Figure.3.4.1.C). In contrast, only a minor fraction of RG cells at the late stage expressed *CRYAB*.

These findings demonstrate the presence of tRG-like cells in ferrets and their similarity to human tRG cells.

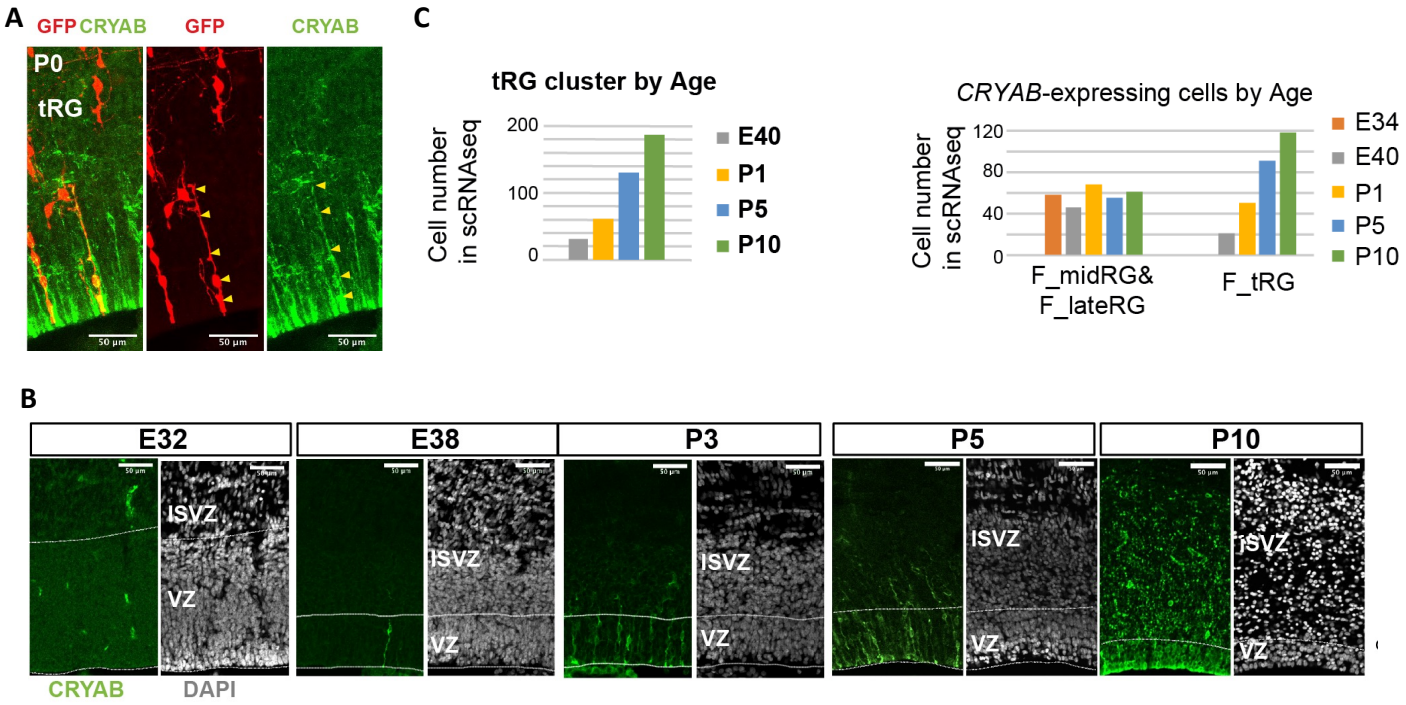

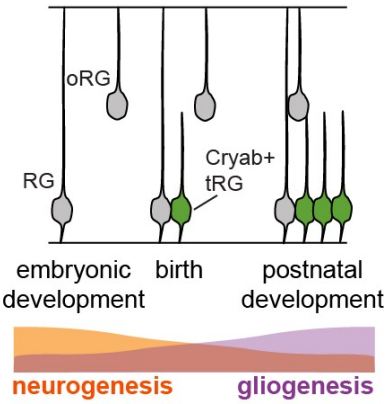

Figure. 3.4.1. *In vivo* identification of tRG through distinct morphology and marker protein expression in developing ferret brain.

A. A representative image showing the cellular features of tRG in VZ at P0, stained for GFP (red) and CRYAB (green). RG cells were sparsely labelled with a GFP-expressing plasmid at E30 via IUE for P0 samples, and at P3 for P5 samples. MAX projection was performed on a 30 µm vibratome section with 5 µm interval for each z-image. Scale bar, 50 µm. **B.** Developmental profile of CRYAB expression in ferret cortices. Immunostaining for CRYAB (green) and DAPI (gray) on cryosections at E32, E38, P3, P5, and P10 (cryosection thickness = 12 µm). A scheme recapitulating the onset and expansion of CRYAB-expressing RG during late embryonic and postnatal stages of the ferret cortical development. **C.** Number of cells in the tRG clustered by age annotated in the ferret transcriptome dataset (left). Number of *CRYAB*-expressing cells in RG clusters of the transcriptome dataset. *CRYAB* expression was not detected at E25. *CRYAB*-expressing cells in midRG and lateRG subtypes remained unchanged in all stages (cell numbers: 58, 46, 68, 55, and 61 at E34, E40, P1, P5, and P10, respectively), while the number of *CRYAB*$^{+}$ tRG cells increased after birth (cell numbers: 0, 21, 50, 91, and 118 at E34, E40, P1, P5, and P10, respectively).

3.4.2. Molecular and cellular features of ferret tRG.

We conducted further investigations into the *in vivo* properties of tRG cells by using cell fate markers from the late neurogenic stage onwards. The majority of CRYAB+ cells in the VZ and SVZ exhibited low levels of TBR2, OLIG2, and KI67 at P5 and P10 (Figure.3.4.2.A), indicating that these cells were largely post-mitotic (KI67-), distinct from intermediate progenitor cells (TBR2+), and not oligodendrocyte progenitor cells (OLIG2+) by P10. These histological findings correlated with our single-cell transcriptome data (Figure.3.4.2.B). Furthermore, a Gene Ontology (GO) term analysis of the ferret tRG cluster revealed gene expression patterns related to the negative regulation of neurogenesis, neuron differentiation, and extracellular matrix organization (Figure.3.4.2.C).

Notably, there was a divergence between humans and ferrets: while conventional RG cells extending radial fibers to the basal surface coexist with tRG cells in the VZ during postnatal development in ferrets (Figure.3.4.2.D), the VZ becomes distinctly separated from the outer subventricular zone (OSVZ) in the human cortex during corresponding stages, as conventional RG cells are absent in the VZ (Nowakowski et al., 2016).

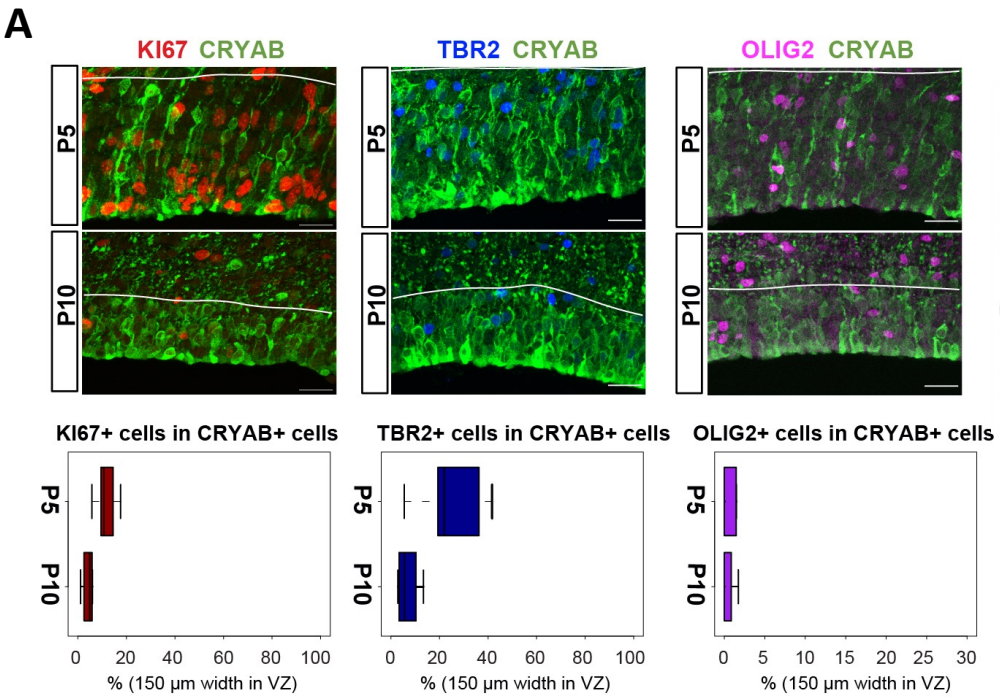

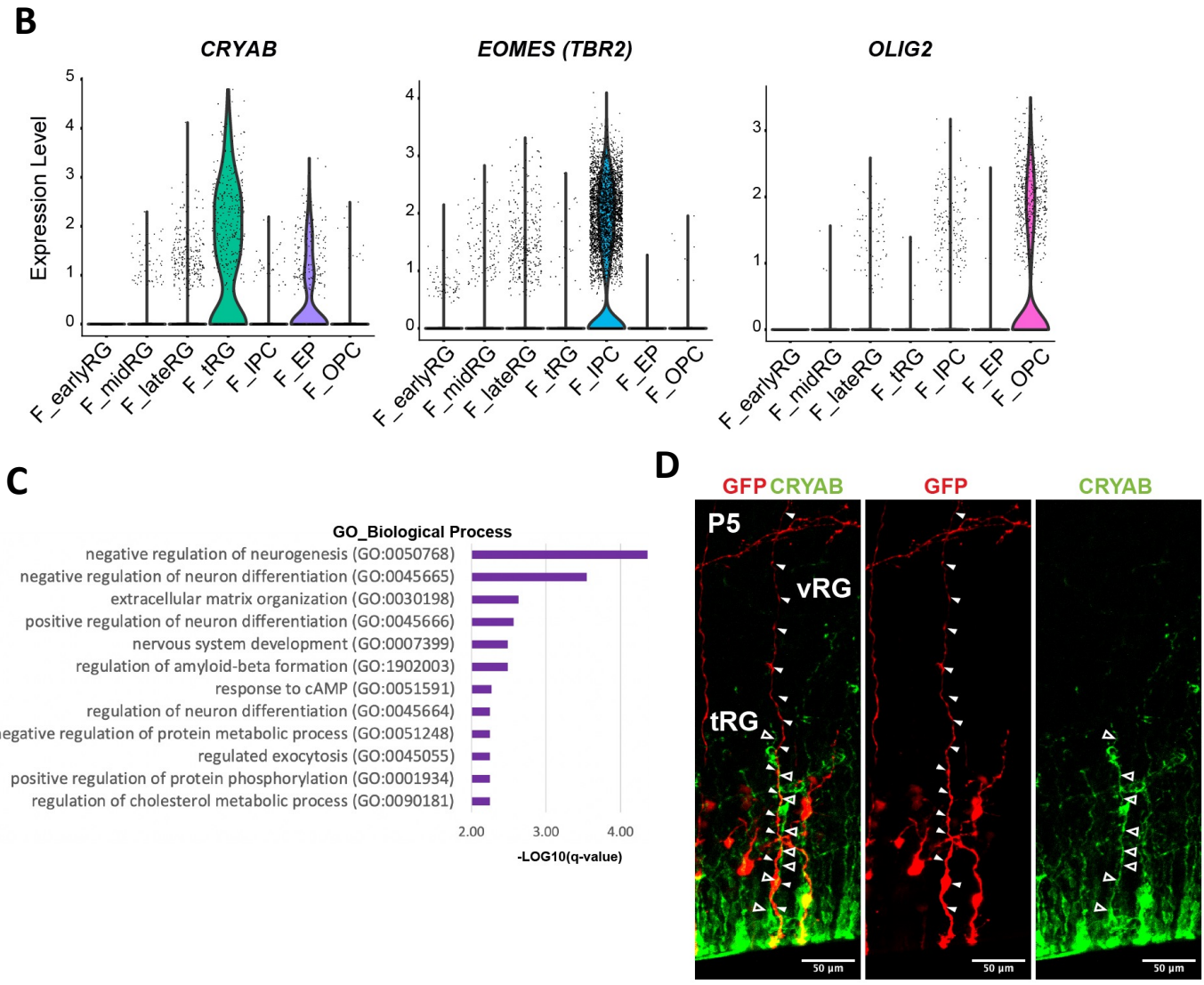

Figure 3.4.2. Molecular and cellular features of ferret tRG.

A. Expression of fate markers in CRYAB$^+$ cells. Representative images taken with a 100X-objective are shown with MAX projection. The border of VZ is shown with a white line. Below each double staining image, quantification of KI67-, TBR2-, or OLIG2-expressing cells among the CRYAB$^+$ cell population in the VZ is shown (n = 2 for P5; n = 2 for P10 for each staining except n = 3 for TBR2 staining). Box and whisker plots indicate ranges (lines) and upper and lower quartiles (box) with the median. Scale bars, 20 µm.

B. Violin plots indicating the normalized expression of *CRYAB* (D), *TBR2* or *EOMES* (E), and *OLIG2*. **C.** Enrichment analysis of Gene ontology (Biological Process) terms associated with tRG markers. **D.** Representative image showing the cellular features of tRG and vRG co-existing in VZ at P5, stained for GFP (red) and CRYAB (green). RG cells were sparsely labelled with a GFP-expressing plasmid at P3 via electroporation. MAX projection was performed on a 30 µm vibratome section with 2.5 µm interval for each z-image at P5. Scale bar, 50 µm.

3.4.3. Observation of generation of tRG by apical divisions of RG sibling cells by timelapse imaging of ferret cortical slices.

In human studies, the mechanism underlying tRG generation has remained elusive, specifically whether it involves the retraction of its basal fiber or originates from apical divisions of vRG cells. To uncover the process of tRG formation in ferrets, we employed time-lapse imaging on cortical slices from ferret embryos. In order to track the sequence of cell divisions within RG lineages, we introduced an EGFP-expressing vector through *in utero* electroporation at E35 or E38, coinciding with the emergence of CRYAB-expressing RG cells. The initiation of time-lapse imaging occurred either at E38 or P0, spanning a three-day interval. Following the imaging, the slices underwent fixation and were subjected to staining for CRYAB and EGFP. The figures and videos of the time-lapse imaging presented in this thesis were generated from experiments performed and processed by Taeko Suetsugu.

In total, we documented four examples wherein tRG cells originated from mitotic progenitor cells. Remarkably, in all these cases, a direct transition from vRG cells to CRYAB+ tRG cells was not observed. Instead, CRYAB+ cells emerged as progeny of apical divisions in mitotic progenitor cells displaying both apical endfoot and a truncated basal fiber. These non-vRG progenitor cells underwent interkinetic nuclear migration (INM) within the VZ, followed by asymmetric division (48:00 in Figure.3.4.3.A; 13:20 in Figure.3.4.3.B), resulting in the generation of a CRYAB+ daughter devoid of the truncated fiber (the deep blue cell) and a non-CRYAB-expressing daughter inheriting the truncated basal fiber (the light blue cell), as depicted schematically in Figure.3.4.3. Subsequently, the CRYAB+ daughter extended a truncated basal process to adopt the tRG morphology (48:00-84:00 in Figure.3.4.3.A; 14:00-60:00 in Figure.3.4.3.B). In two out of the four examples, the mitotic mother cells of tRG (the deep blue cell, see also Supplementary movie 1) were sibling cells of a dividing vRG characterized by a full-length radial fiber (the pink cell in Figure.3.4.3.A). In the remaining two cases, technical constraints hindered the tracking of tRG mother cell genesis. Taken together, our findings propose that tRG cells originate through apical asymmetric divisions of distinct apical intermediate progenitor cells featuring a truncated basal fiber (Tsunekawa et al. from Matsuzaki Laboratory in preparation). Notably, it is plausible that these progenitors, responsible for generating tRG cells asymmetrically, may already express CRYAB. Evidently, a subset of CRYAB-expressing tRG cells (approximately 20%) exhibited mitotic activity, followed by a subsequent decline in post-mitotic phases (Figure 3.4.2.A).

Given the infrequent labeling of the tRG cell population and the limited presence of mitotic tRG cells, one could speculate that this cell type either divides slowly or maintains a more quiescent state. This notion could potentially elucidate the modest rate of tRG labeling via *in utero* electroporation.

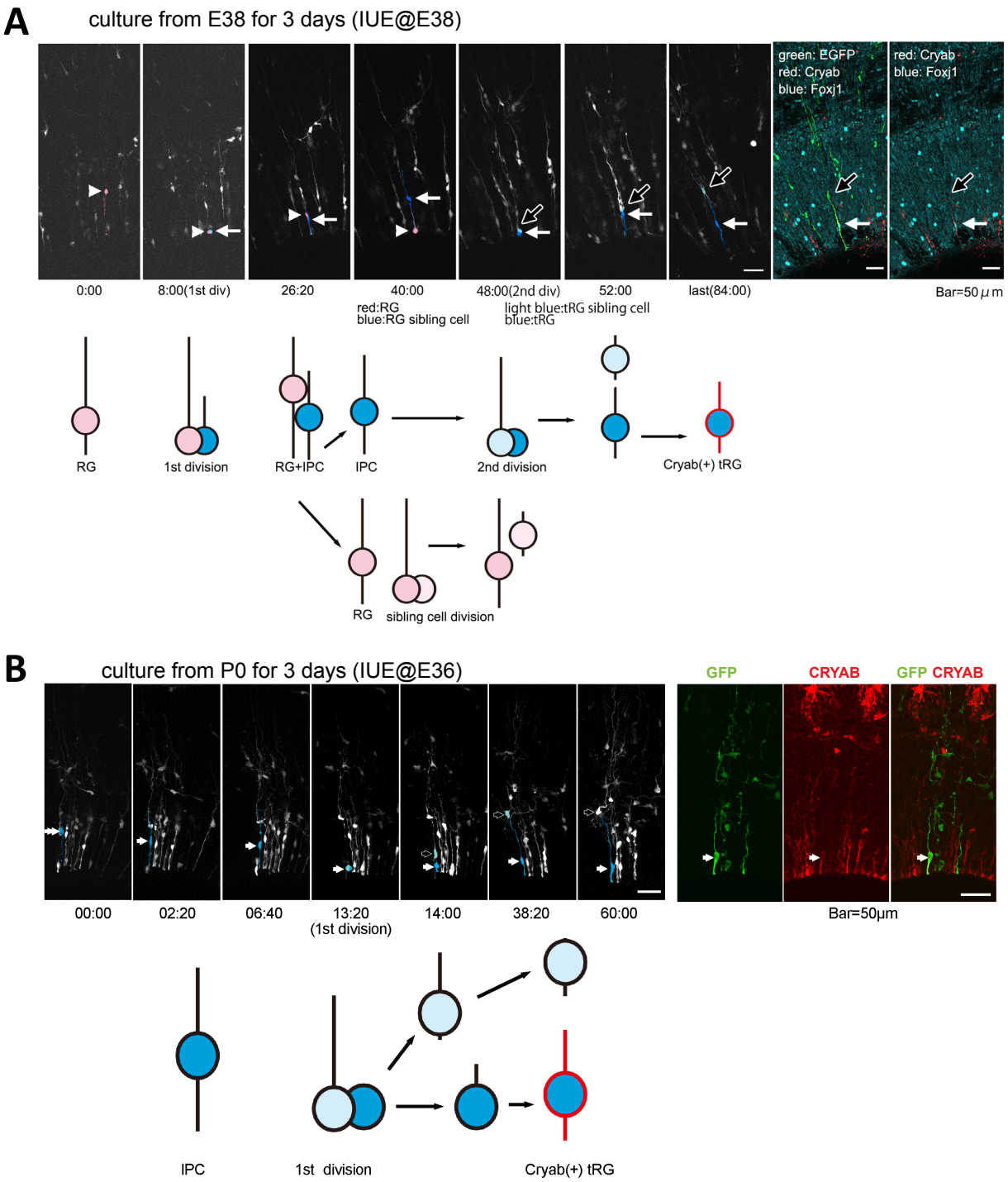

Figure 3.4.3. Generation of tRG by apical divisions of RG sibling cells by timelapse imaging of ferret cortical slices.

A. Sequential snapshots of time-lapse imaging of an EGFP-labeled vRG cell, which produced a parental RG that asymmetrically divided into tRG at the end of the imaging. The time below each snapshot strip indicates the time (hour) passed after the slice culture was started. The white arrowheads indicate ancestral vRG (pink). The vRG underwent a first division at 8:00, generating a daughter cell that underwent an interkinetic nuclear migration (8:00–48:00), and generated a

CRYAB$^+$ daughter (blue) by an asymmetric division (48:00). Open arrows indicate the other daughter (light blue). Below the snapshots, a schematic of the time-lapse imaging is shown. Colors represent cells as in snapshots. The cultured slice was fixed at 84:00 and stained for EGFP (green), CRYAB (red), and FOXJ1 (light blue). EGFP staining shows that CRYAB$^+$ FOXJ1$^+$ cell has a short basal fiber. Scale bar, 50 μm. **B.** Time-lapse imaging of an EGFP-labeled RG forming a tRG. An apically attached mitotic RG (white arrows, blue cell body) with a short basal fiber produced a tRG cell (blue). Sequential snapshots showing that the mitotic RG forming tRG through an apical division at 13:20. tRG sibling cells are marked by light blue color and open arrows. Below snapshots, a schematic representation of tRG formation is shown. Cells are marked by the same colors as in snapshots. Immunostaining of a cryostat section from a fixed slice stained for CRYAB (red) and EGFP (green) at the end of the timelapse imaging.

3.4.4. BMP signaling might be involved in the induction of tRG cells.

To elucidate potential signaling mechanisms of tRG formation, we performed a pathway analysis by KEGG pathways. Notably, the expression of genes associated with the Transforming Growth Factor-beta (TGF-β) signaling pathway (i.e. *SMAD1*, *ID1*, *ID2*) and tight junctions (i.e. *ITGB1*, *JUN*), observed in ependymal cells, was upregulated within ferret tRG cells (Figure.3.4.4.A). Previous reports have shown that, Bone Morphogenetic Protein (BMP), a member of the TGF-β family, was implicated in the divergent development of neural progenitors and ependymal cells within the ventral telencephalon (see results 3.5.; Omiya *et al*, 2021). These findings led us to examine BMP's involvement in tRG formation.

We immunostained phosphorylated SMAD1/5 as an indicator of TGF-β signaling, including BMP-mediated pathways, and found an overlap with CRYAB-expressing cells in VZ (Figure.3.4.4.B). We then focused on investigating the role of BMP2 since it is a major regulator of this phosphorylation. For this purpose, cortical slices were exposed to BMP2 added into the culture media. The majority of these experiments were performed by Taeko Suetsugu. Administering BMP2 to postnatal cortical brain slices at P0 resulted in the increase of CRYAB expression within 24 hours, when cultivated in serum-free media (Figure.3.4.4.C). Contrarily, the application of LDN-193189, a BMP inhibitor, did not evoke any noticeable changes in either the CRYAB+ cell population. These outcomes suggest the potential positive role of BMP2 in tRG formation and/or the modulation of CRYAB expression.

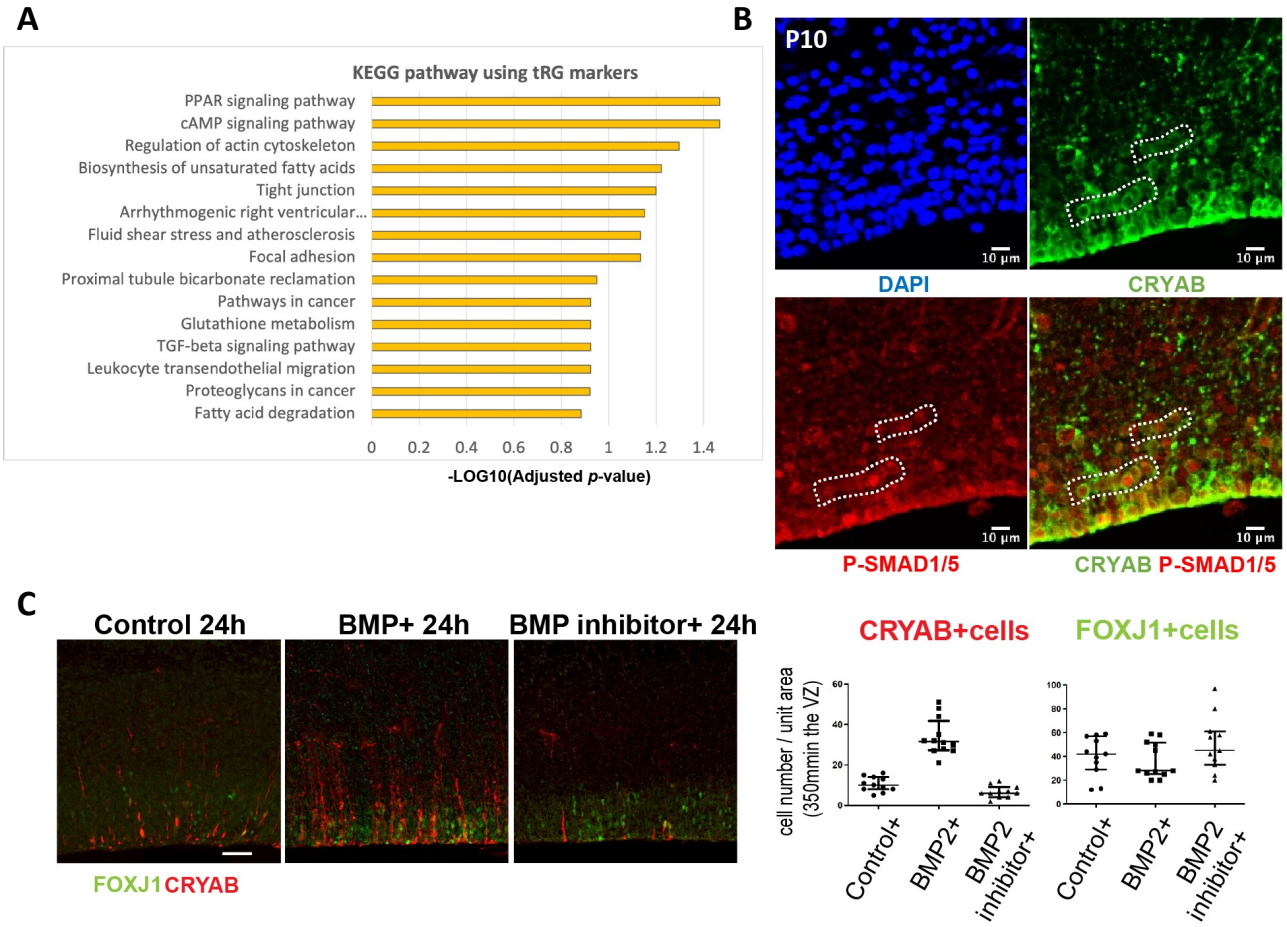

Figure. 3.4.4. BMP signaling might be involved in the induction of tRG cells.

A. KEGG pathway (KEGG Human 2021) analysis associated with tRG markers. **B.** Immunostaining for CRYAB (green) and phosphorylated-SMAD1/5 (red) showing an overlapping expression P-SMAD1/5 in CRYAB-expressing cells in VZ of P10**. C.** Immunostaining for FOXJ1 and CRYAB after a postnatal administration of BMP2 or its inhibitor, LDN-193189 to P0 cortical brain slices (left). Quantification of CRYAB+ and FOXJ1+ cells are shown on the right. The experiment was performed in two independent replicates, on at least 5 sections per experiment. Each point reflects a section, and the specific shape of the points are assigned to different conditions (round for control, square for BMP2 administration, triangle for BMP2 inhibitor). The scatter plot shows the results for the second experiment. Dunnett's multiple comparisons test was used for statistical analyses of the quantification results. Each experiment showed a significant increase in CRYAB+ cells 24 hours after BMP2 administration compared with the control, whose adjusted *p*-value was <0.0001 for both experiments, while the inhibition of BMP2 did not affect CRYAB expression (inhibitor vs control; adjusted *p*-value, 0.9253 and 0.2702, respectively for two serial experiments).

3.4.5. The lack of tRG formation in human organoids.

Human cortical organoids serve as a valuable tool to understand how the brain develops (Eiraku *et al*, 2008). It's important to figure out whether human organoids can be a good model to study tRG development. To explore this, we analyzed two distinct datasets of cortical organoids (Bhaduri et al., 2020; Herring *et al*, 2022). We focused on CRYAB-expressing cells on Bhaduri dataset where organoids were derived from four distinct cell lines (Figure.3.4.5.A). Surprisingly, we didn't find any of CRYAB+ cells in the organoids that matched tRG cluster in the developing human brain tissues (Bhaduri et al., 2020; Figure.3.4.5.B). We also couldn't find any CRYAB cells in the dataset from Herring et al., 2022 (Figure.3.4.5.C). This suggests that the types of cells similar to tRG cells might be missing in the organoid datasets that are available.

The plausible explanation for this discrepancy could lie in the absence of extrinsic cues inherent to organoids, such as those emanating from the choroid plexus or cerebral fluid, which are absent in the organoid cultures. One may speculate that BMPs exert influence the formation and maintenance of the tRG cells.

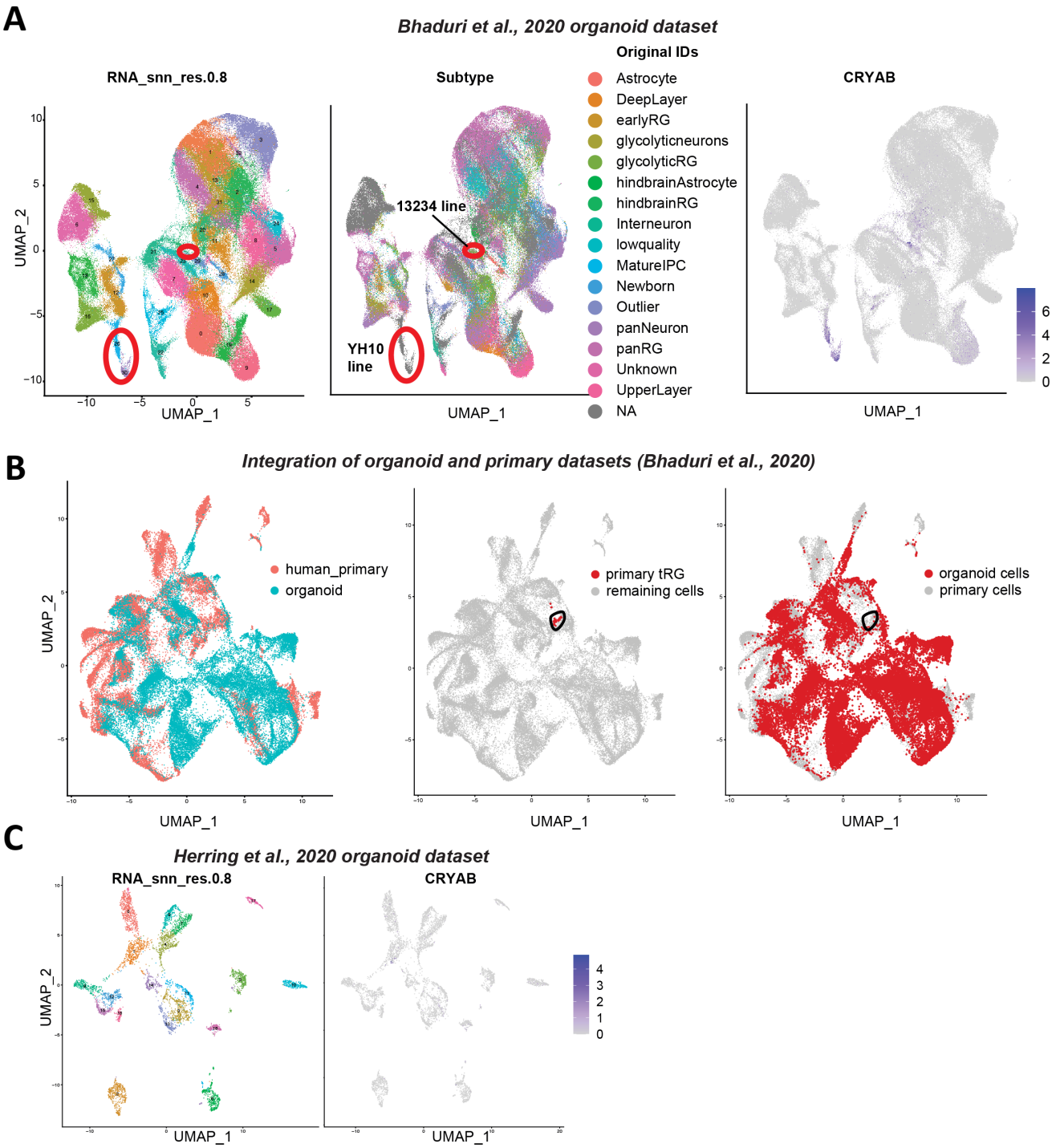

Figure. 3.4.5. The lack of tRG formation in human organoids.

A. UMAP visualization of human organoid-driven cells colored by clusters (left), the original cluster annotations (middle) or by the normalized expression level of *CRYAB* (right). Human organoid dataset from Bhaduri et al., 2020 was used. Bhaduri dataset contained organoids generated from 4 different lines, which showed a variability in terms of cell distribution on UMAP while overall temporal and differentiation axes were recapitulated. Red circles on UMAP highlight the group of cells expressing *CRYAB*. *CRYAB* expression was restricted to two out of four cell

lines. CRYAB was expressed in clusters 26 and 30 enriched in the YH10 line, and cluster 29 enriched in the 13234 cell line. **B.** UMAP visualization of integrated primary and organoid datasets from Bhaduri et al., 2020. Cells are colored by the originated dataset (left), primary tRG cluster (middle) or organoid dataset (right). Black circles were used to indicate the overlap of the region where human primary tRG was found. Human tRG did not overlap with organoid cells. We found that CRYAB-expressing organoid clusters 26 and 30 overlapped with "oRG/astrocyte" clusters of primary tissues. **C.** UMAP visualization of cells derived from Herring et al., 2022 human organoid dataset, colored by clusters (left) or by the normalized expression level of *CRYAB* (right).

3.5. tRG possesses ependymal and astrogenic potential during ferret cortical development.

3.5.1. Formation of epithelia-like belt of nuclei-aligned RG cells in the basal side of ventricular zone prior to ependymal layer formation on the apical surface.

In a parallel exploration of our transcriptome data (see results 3.5.3), an intriguing pattern began to emerge, which is the relationship between nuclear alignment and the onset of CRYAB expression in radial glial (RG) cells (Figure.3.5.1 and Figure.3.4.1, respectively). From P5 onwards, we observed PAX6+ nuclear clusters aligning in the basal side of the VZ, in parallel with the ventricular surface (Figure.3.5.1.A, highlighted between two arrowheads). Most of these cells expressed CRYAB (Figure.3.5.1.B). As we tracked these cells over time, their cell bodies ultimately settled on the apical surface (Figure.3.5.1.C).

This observation of a gradual transformation in the VZ coinciding with the emergence of tRG, in turn, suggests a profound connection between tRG cells and the eventual fate of ependymal cells, and led us to hypothesize that the function of tRG might be at least to produce ependymal cells in Gyrencephalic species.

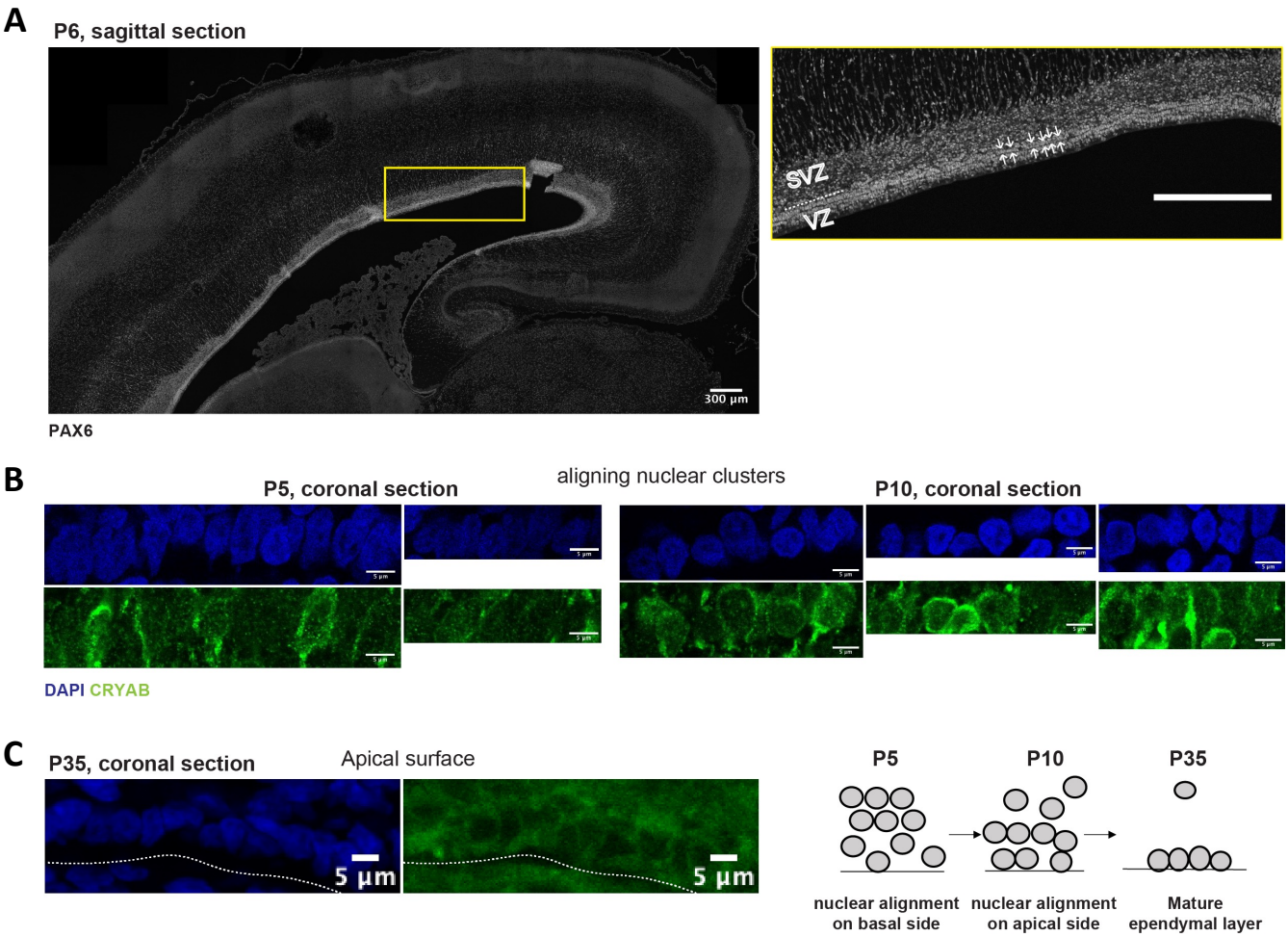

Figure 3.5.1. Formation of epithelia-like belt of nuclei-aligned RG cells in the basal side of ventricular zone prior to ependymal layer formation on the apical surface.
A. Immunostaining for PAX6 on sagittal sections at P6 ferret cortex. On right, the cropped image of the selected area (yellow) represents the the nuclear alignment on the boundary between VZ and SVZ. Scale bar, 300 μm. **B.** The expression of CRYAB (green) in aligning cells on cropped images in VZ by immunostaining ferret cortex at P5 (left), and P10 (right). Scale bar, 5 μm. **C.** The expression of CRYAB (green) on the ependymal layer on cropped images in VZ by immunostaining ferret cortex at P35. Scale bar, 5 μm. The schematic on right represents the observations in A and B over the course of the ferret brain development.

3.5.2. Pseudotime trajectory analysis predicted temporal fates of RG cells.

In order to decipher the relationships among diverse cortical progenitor cells within the developing ferret brain, with a particular focus on elucidating the origin and developmental trajectories of ferret tRG cells, we performed pseudotime analysis using the Monocle 2 framework. This analysis involved arranging single cells ranging from E25 to P10 along a trajectory, based on their transcriptome profiles in an unbiased manner. Cells originating from non-cortical lineages such as interneurons, microglia, and endothelial cells, along with excitatory neuron clusters, were excluded from the analysis. Subsequently, a representative subset of 6,000 single cells was randomly selected from the remaining population for subsequent analysis. This approach was validated through successful projection of the developmental trajectory within the dorsal cortex, where the selected cells were positioned along the trajectory from earlier to later developmental stages (Figure.3.5.2.A-C).

The pseudo-lineage analysis delineated a trajectory characterized by three branching points that gave rise to seven distinct branches. Major cell types were attributed to each branch based on UMAP clustering, with the nomenclature of each branch being reflective of the dominant cell types occupying them (Figure.3.5.2.D). The initial branching point marked the genesis of the neuronal differentiation lineage (branch 1), followed by the emergence of the oligodendrocyte lineage (branch 4) at the second branching juncture. The third and final branching point resulted in the bifurcation of the ependymal lineage (branch 6) and the astroglial lineage (branch 7), a classification described in detail subsequently.

Progenitor cells from early embryonic stages (beginning at E25) were situated at the trajectory's inception, predominantly diverging into the neurogenic state. RG cells spanning from E34 to P1 exhibited the capacity to generate both neurogenic and gliogenic trajectories (Figure.3.5.2.B). Following birth, neurogenesis experienced a gradual decline, whereas gliogenic processes exhibited steady progression. The arrangement of marker gene expression profiles (i.e. *FOXJ1*, *PTN*) and cellular clusters along the pseudotime trajectories indicated that the terminal branching distinctly segregated the NPC type 3 cells (state 5) into ependymal and astroglial lineages (Figure.3.5.2.C-D).

Notably, the tRG cell population was found distributed across three distinct states along the trajectory (Figure.3.5.2.E): the NPC3 state (predominantly spanning E40 to P1), the astrogenic state (encompassing P1 to P10), and the ependymal state (encompassing P5 to P10). These data collectively suggested that tRG cells emerged prenatally (potentially from late RG cells, as discussed earlier) and subsequently assumed the role of precursors for both ependymal and astroglial lineages within the ferret cortex.

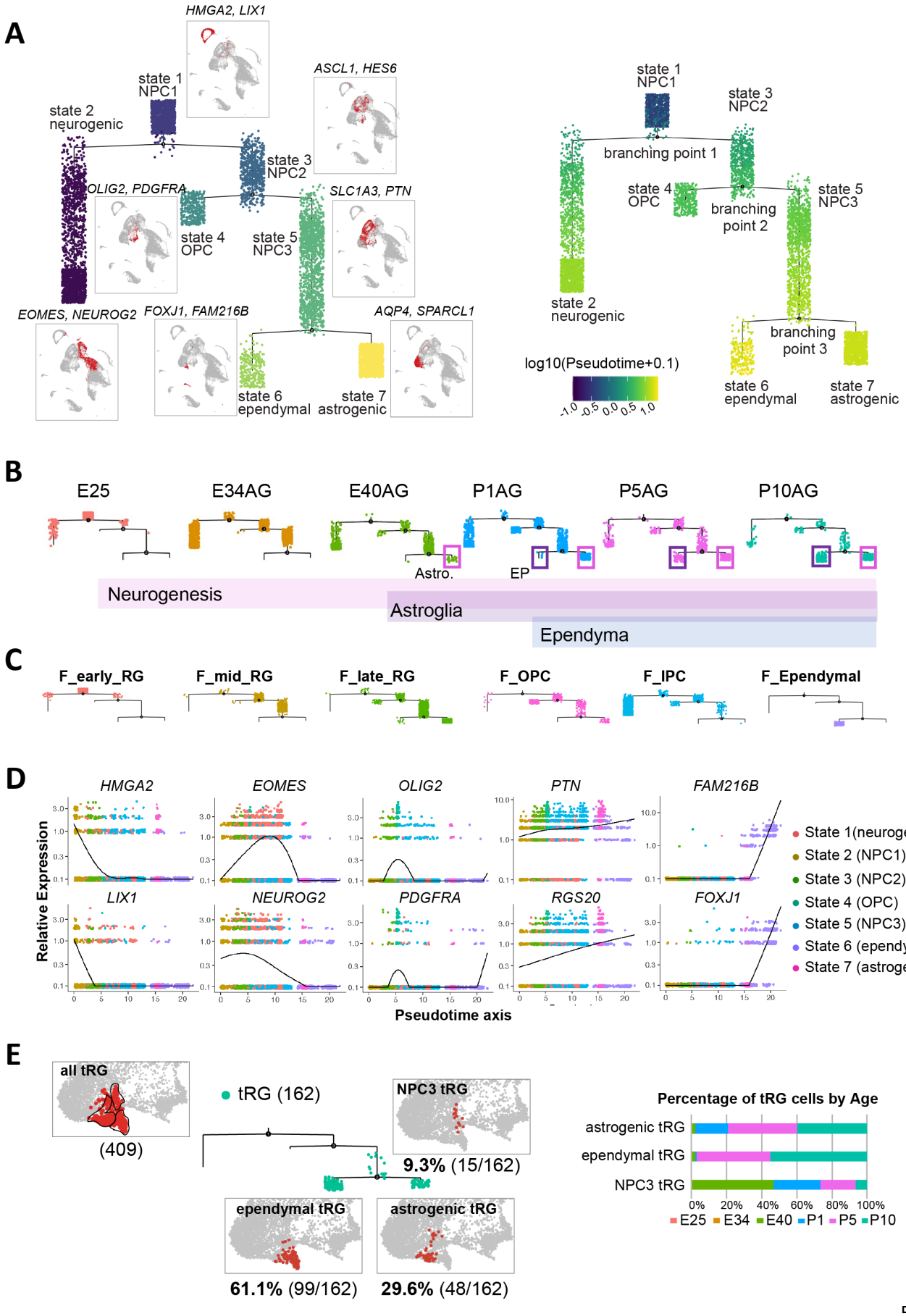
A
HMGA2, LIX1
ASCL1, HES6
state 1
NPC1
state 2
neurogenic
state 3
NPC2
OLIG2, PDGFRA
SLC1A3, PTN
state 4
OPC
state 5
NPC3
EOMES, NEUROG2
FOXJ1, FAM216B
AQP4, SPARCL1
state 6
ependymal
state 7
astrogenic
state 1
NPC1
state 3
NPC2
branching point 1
state 4
OPC
branching
point 2
state 5
NPC3
state 2
neurogenic
branching
point 3
state 6
ependymal
state 7
astrogenic
log10(Pseudotime+0.1)
-1.0 -0.5 0.0 0.5 1.0
B
E25
E34AG
E40AG
P1AG
P5AG
P10AG
Astro.
EP
Neurogenesis
Astroglia
Ependyma
C
F_early_RG
F_mid_RG
F_late_RG
F_OPC
F_IPC
F_Ependymal
D
HMGA2
EOMES
OLIG2
PTN
FAM216B
LIX1
NEUROG2
PDGFRA
RGS20
FOXJ1
Relative Expression
Pseudotime axis
State 1(neurogenic)
State 2 (NPC1)
State 3 (NPC2)
State 4 (OPC)
State 5 (NPC3)
State 6 (ependymal)
State 7 (astrogenic)
E
all tRG
(409)
tRG (162)
NPC3 tRG
9.3% (15/162)
ependymal tRG
astrogenic tRG
61.1% (99/162)
29.6% (48/162)
Percentage of tRG cells by Age
astrogenic tRG
ependymal tRG
NPC3 tRG
0% 20% 40% 60% 80% 100%
E25 E34 E40 P1 P5 P10

Figure. 3.5.2. Pseudotime trajectory analysis predicted temporal fates of RG cells.
A. Pseudo-time trajectory tree of progenitor cells in the ferret developing cortex (assembled with Monocle v2). The cells are colored by their state (branch; left) or by their pseudotime score (right). Cell types representing each state and their gene markers are shown next to each state (left). **B.** Trajectory trees split by collection stages (AG samples are shown). The onset of astroglia state and ependymal state is highlighted. **C.** Trajectory trees split by the indicated cell type. **D.** Distribution of cells expressing marker genes for representative cell states along the linear pseudotime axis. Y-axis indicates the relative normalized expression of the markers in all cells. **E.** Distribution of tRG cells along the tree and tRG-focused UMAP visualization (left). The tRG cells (n = 162) were found on the three states, NPC3 (9.3%; 15 cells), ependymal-tRG (61.1%; 99 cells), and astrogenic-tRG (29.6%; 48 cells). Composition of the three types of tRG by the collection stage (AG and T samples are combined) is shown by the bar plot on right. No tRG cells were collected from E25 and E34.

3.5.3. Ependymal fate markers were expressed in tRG cells *in vivo* from the peak stage of tRG abundance.

To examine the possibility that tRG cells give rise to both ependymal cells and astroglial populations, the differentiation of tRG cells into ependymal cells was first assessed via immunostaining, focusing on the ependymal marker FOXJ1, a crucial regulator of ciliogenesis (Figure.3.5.3.A). The immunostaining results demonstrated a progressive co-expression of FOXJ1 and CRYAB in tRG cells, with up to 90% of CRYAB+ cells exhibiting FOXJ1 expression by P10 (Figure.3.5.3.B). A similar trend was observed in the transcriptome data, wherein the fraction of *CRYAB* and *FOXJ1* double-positive cells increased in the *CRYAB*+ cell subset from P1 to P10 in the tRG cluster, while other RG clusters displayed consistently low levels of *CRYAB* expression (Figure.3.5.3.C). Additionally, differentiating ependymal cells were confirmed to be situated within the ventricular zone (VZ) by P14, characterized by short basal fibers and eventual settlement of cell bodies on the apical surface (Figure.3.5.3.D). These observations collectively suggest that a subset of tRG cells progressively upregulates *FOXJ1* expression, signifying their adoption of an ependymal cell fate during postnatal development. Moreover, the expression of Adenylate Cyclase III, detectable in both primary and multi-cilia, indicated a postnatal progression of ciliogenesis, ultimately resulting in the formation of multi-ciliated ependymal cells on the ventricular surface of the ferret cortex by P35 (Figure.3.5.3.E).

Furthermore, a subset of tRG cells pertains to state 7 (astrogenic state) within the pseudo-time trajectory. To explore the differentiation of these tRG cells into astroglial cells, we chose *FOXJ1* as an ependymal marker and *SPARCL1* as an early astroglial marker (Liu et al., 2022). Notably, while *SPARCL1* is expressed across all states generated by NPC3, its expression peaks in the astroglial tRG subgroup, whereas *FOXJ1* expression is predominantly found in ependymal tRG (Figure.3.5.3.F). Taken collectively, our analyses suggest that tRG cells possess the capacity to adopt both ependymal and astroglial fates, which requires further lineage tracing examination *in vivo*.

Taken all together, the increasing prevalence of CRYAB-FOXJ1 double-positive cells within the tRG cluster implies a pivotal role played by CRYAB+ tRG in the formation of ependymal cells. Furthermore, the pronounced nuclear alignment observed in differentiating ependymal cells suggests a unique developmental program, with these cells undergoing a series of changes that culminate in their eventual settling on the apical surface with truncated basal fibers.

This relationship between nuclear alignment and CRYAB expression opens the door to intriguing avenues of research, offering novel insights into the connection between tRG cells and the remarkable journey towards ependymal fate within the developing neural landscape. To get insights on this by examining the function of CRYAB, we attempted to knock-out CRYAB in RG by combining Crispr/Cas9-mediated and *in utero* electroporation over two years but consistently failed to specifically knock-out CRYAB among electroporated cells.

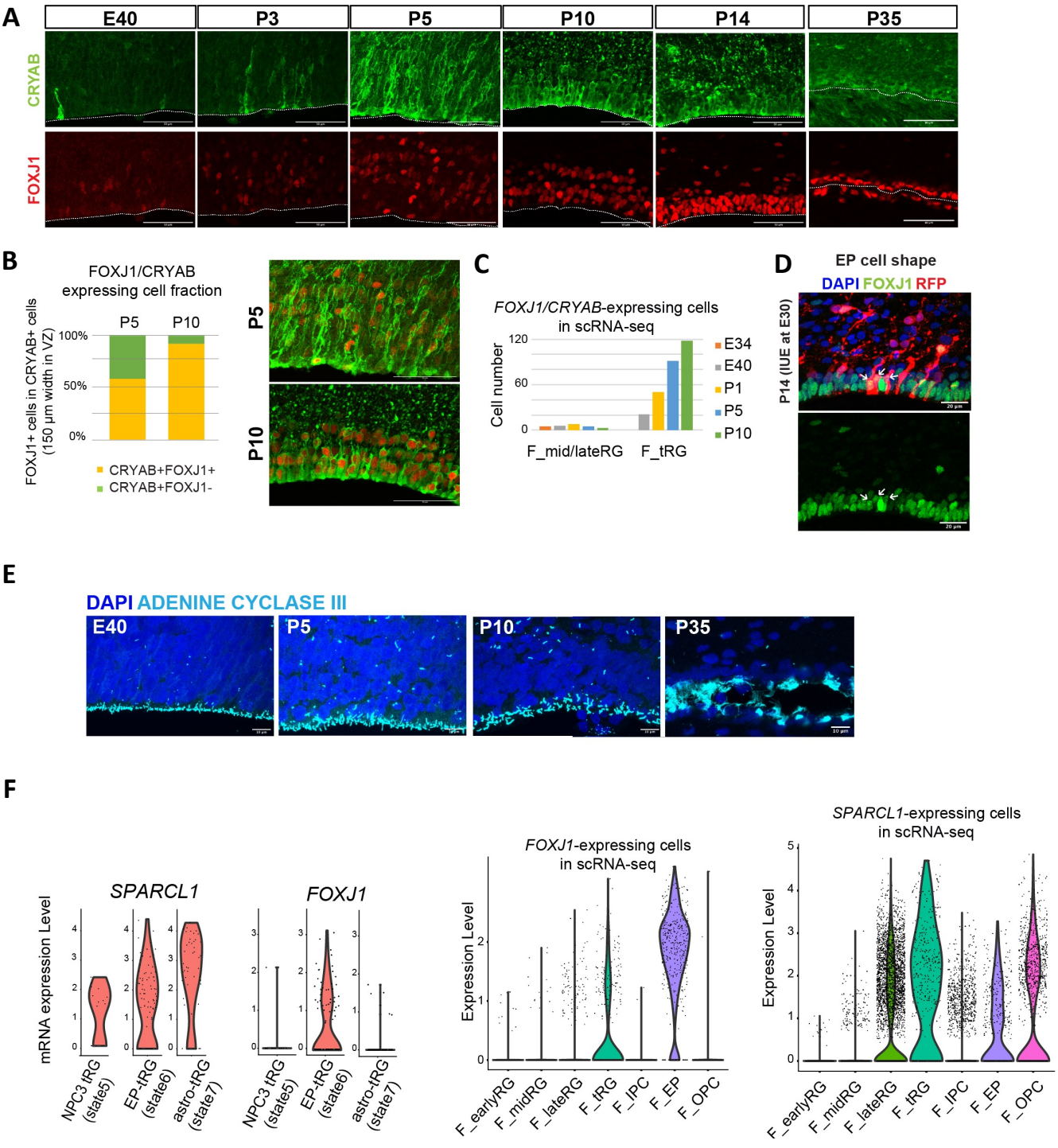

Figure.3.5.3. Ependymal fate markers were expressed in tRG cells *in vivo* from the peak stage of tRG abundance.
A. Immunostaining of 12 μm cortical cryosections with CRYAB (green) and FOXJ1 (red), focusing on the VZ at E40, P3, P5, P10, P14, and P35. Scale bar, 50 μm. **B.** Percentage of FOXJ1 expression in CRYAB-expressing cells (n = 3 for P5; n = 2 for P10; Wilcoxon rank sum test *p*-value = 1.749e-05). Images with merged channels in A are shown with the same color codes, antibodies and scale bars as A. **C.** Number of cells expressing both *CRYAB* and *FOXJ1* in the mid and late RG, or tRG clusters (with unique molecular identifier counts higher than 0.25). Colored bars indicate the stages of sample collection. *CRYAB*- and *FOXJ1*-expressing cells increased over time only in the tRG cluster. **D.** Cortical origin and shape of FOXJ1-expressing ependymal cells indicated with white arrows. Staining for FOXJ1 at P14 after labeling cortical progenitors with an mCherry-expressing vector via IUE at E30. The maximum projection images with 1 μm z-step size are shown. Cryosection thickness = 12 μm; scale bar = 20 μm. **E.** Onset of ciliogenesis in the developing cortex of ferrets, shown via staining for ADENINE CYCLASE III (cyan) along the VZ surface at E40, P5, P10, and P35. Scale bars = 10 μm. **F.** Normalized expression of *SPARCL1* and *FOXJ1* in each cell in ferret tRG subclusters separated by the pseudo-time trajectory analysis (left). Normalized expression of *SPARCL1* and *FOXJ1* in the major cell types of progenitors in our scRNA-seq data in ferrets (right).

3.5.4. Molecular signature of tRG and its potential ependymal and astroglia fates were comparable between the two species.

To evaluate the plausible ependymal and gliogenic capabilities within human tRG cells, similarly to those observed in ferrets, our strategy involved two aspects: (1) the selection of a recently published human dataset encompassing cells at GW25 with high numbers of tRG cells as compared to preceding datasets (Bhaduri et al., 2021), and (2) a refined focus on NPC populations, thereby excluding neurons and other cellular categories from the analytical scope.

The integration of the ferret and human datasets using only NPC clusters created a predominant distribution of human and ferret tRG cells within three distinct clusters: 7, 21, and 28 (Figure.3.3.3.B, Figure.3.5.4.A). While the human tRG were enriched in integrated cluster 7, ferret tRG cells were the most enriched in cluster 28, followed by cluster 21 (Figure.3.5.4.B).

The cluster 7 exhibited a transcriptomic expression profile similar to that exhibited by late RG cells, characterized by pronounced expression of RG-specific marker genes such as *APOE*, *FABP7*, *NOTCH2*, and *DBI* (Figure.3.5.4.C). This profile implied that tRG cells within cluster 7 assumed a late RG-like state – a state corresponding to cells in the NPC 3 branch within the pseudo-temporal trajectory described previously. In contrast, the transcriptomic signatures of clusters 21 and 28 were marked by higher expression levels of marker genes typifying astrocyte (*GFAP* and *AQP4*) and ependymal (*FOXJ1* and *CRYAB*) identities, respectively.

The validation of this classification of tRG cells into the three major clusters post-integration was substantiated through a comparison between the clustering pattern of ferret tRG cells within the integrated dataset and the categorization of these cells within the pseudo-temporal trajectory analysis (Figure.3.5.4.E). Here, we found a similar distribution pattern of three distinct tRG subtypes between humans and ferrets on UMAP (Figure.3.5.4.D). Strikingly, these two distinct analytical approaches yielded largely similar outcomes regarding the classification of ferret tRG cells, providing robust evidence for the reliability of the tRG fate bifurcation. Our findings suggest the parallel potential of tRG cells across both human and ferret contexts to give

rise to astrocytes and ependymal cells. Notably, the distribution of the three tRG subtypes between the human and ferret datasets were different, with increased occurrences of ependymal and gliogenic tRG cells in ferrets, and dominance of late RG-like tRG cells within the human dataset (Figure.3.5.4.B). This divergence is likely attributed to developmental disparities between the two datasets. At the moment, a human dataset enriched with mature ependymal cells is absent due to ethical reasons since the multiciliated ependyma seems to appear not prior to GW30 (A.J. *et al*, 2014), which limits the access for a comparison of ependymal lineage between humans and ferrets.

Taken all together, *in silico* analyses led to the prediction that tRGs in humans likely acquire both ependymal and astrogenic fates during cortical development. This prediction was based on the comparison of human and ferret transcriptome datasets, implying potential functional similarities in tRGs across species. In ferrets, tRGs were found to acquire both ependymal and astrogenic fates, indicating their role in the formation of adult ventricles. The presence and proposed roles of tRGs in Gyrencephalic mammals suggest that they contribute to the architectural basis of brain expansion, which is more limited in Lissencephalic mammals, such as mice (see Discussion).

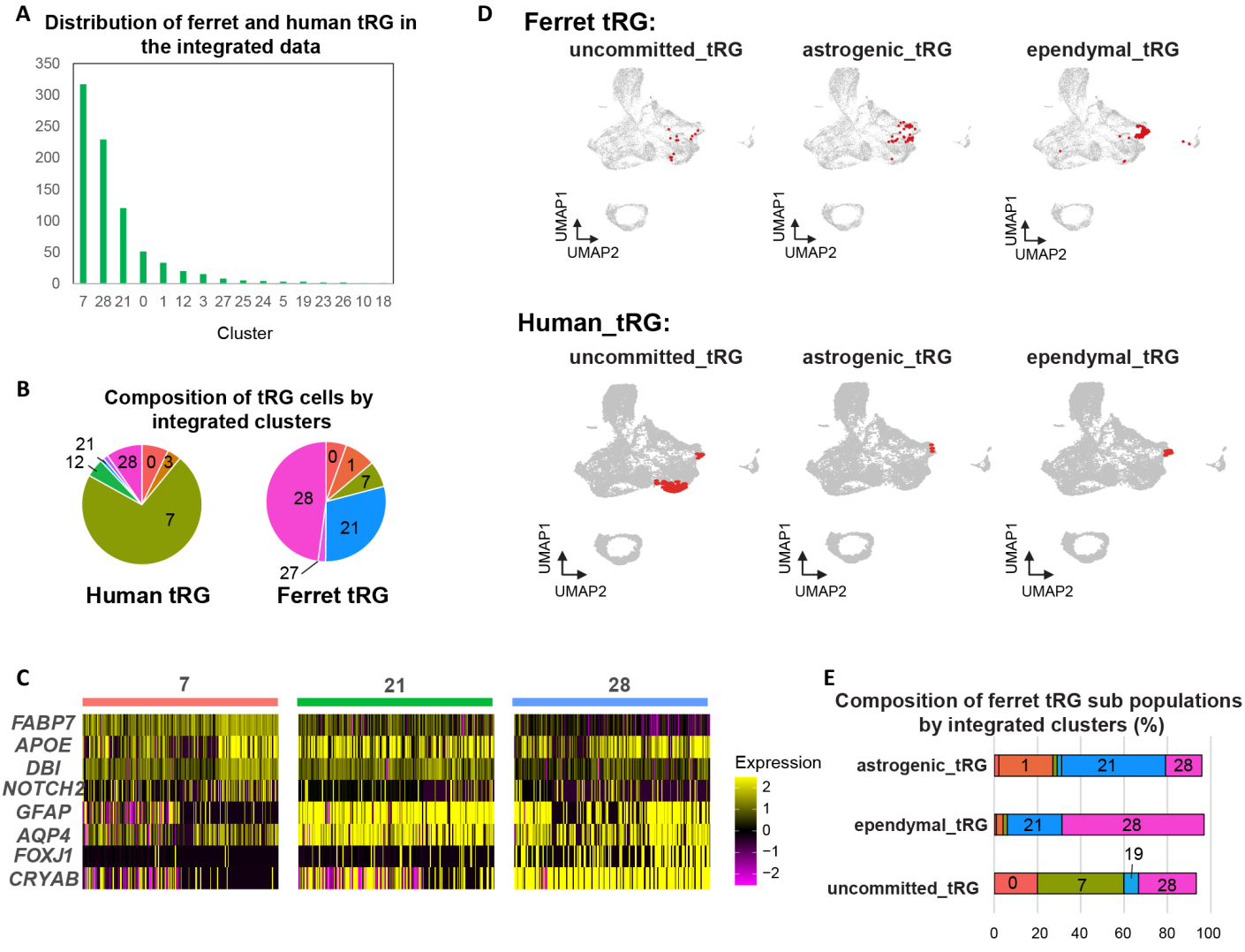

Figure.3.5.4. Molecular signature of tRG and its potential ependymal and astroglia fates were comparable between the two species.
A. Distribution of human and ferret tRG in the integrated dataset. The number in the X-axis indicates the cluster number identified by the UMAP in Figure.3.3.3B. **B.** Distribution of human tRG cells (left) and ferret tRG cells (right) in the integrated dataset. Human and ferret tRG were identified from the separated dataset. The numbering corresponds to cluster numbers in the integrated clustering of human and ferret datasets (A). **C.** Expression levels of the subtype maker genes in the three tRG-enriched clusters (7, 21, and 28). Marker enrichment is consistent with the presumptive identification of tRG subtypes according to pseudotime trajectory analysis. **D.** Identification of three tRG subtypes in ferrets (top) and humans (bottom). The red dots highlight the indicated tRG subtypes named after pseudotime trajectory analysis: presumptively "uncommitted", "astrogenic" and "ependymal". **E.** Percentage of ferret tRG subtypes (identified by the pseudo-time analysis) in the clusters of integrated dataset. A major cell population of each of the 3 ferret tRG subtypes (classified by the pseudo-time analysis), more or less, belongs to a single cluster in ferret-human integrated clustering; astrogenic tRG corresponds to cluster 21; ependymal tRG to cluster 20; uncommitted tRG to cluster 7.

Chapter 4

DISCUSSION

4.1. Transcriptome of ferret cortical cells are resolved at temporal and single-cell levels.

The study of Neural Progenitor Cells (NPC) diversity significantly contributes to comprehend the development of the cerebral cortex in Gyrencephalic mammals, including Primates and Carnivora. This complex process relies on the interplay among various NPC, and gaining insights into their diversity becomes crucial for unraveling the underlying mechanisms of brain development and evolution.

Furthermore, this knowledge has implications for understanding neurological disorders and brain-related pathologies. By exploring the heterogeneity of NPC at the cellular and molecular levels, we achieved a deeper understanding of the formation and maturation of the cerebral cortex from distinct progenitor subtypes, which can lead to advancements in the fields of neuroscience and developmental biology.

4.2. Ferrets as a Model for studying corticogenesis in Gyrencephalic species.

Ferrets serve as an excellent model for studying corticogenesis in Gyrencephalic mammals due to their neuroanatomical similarities with primate species including humans. Furthermore, the feasibility of experimental manipulations and the availability of genetic tools make ferrets an ideal candidate for investigating cortical development in a laboratory setting. In this study, we took advantage of this by performing live imaging of ferret cortical slices, and *in utero* electroporation, to reveal the formation of tRG cells by asymmetric division, and to follow the fate of RG lineages, respectively. Although we have failed to apply knock-out strategies into our system *in vivo*, leveraging the advantages of the ferret model by applying appropriate methodologies for functional studies can enhance our understanding of neural progenitor cell dynamics and their contributions to cortical expansion, shedding light on fundamental aspects of brain development.

4.2. Identification of truncated radial glia (tRG) in ferrets and its significance.

In the course of this PhD study, we identified truncated radial glia (tRG) in ferrets, a neural progenitor cell subtype that had been previously described in humans but remained poorly understood. This finding holds significant implications for our understanding of brain development in Gyrencephalic mammals. The identification of tRGs in ferrets provides an opportunity to investigate their role and function during corticogenesis, unraveling the mechanisms that underlie the formation of the cerebral cortex. By elucidating the properties and contributions of tRGs, we may gain insights into their potential involvement in neurological diseases and brain disorders.

The identification and characterization of tRGs and their proposed common and crucial roles in the formation of adult ventricles present intriguing insights into the process of brain expansion in Gyrencephalic mammals. These findings provide an architectural basis for understanding the mechanisms that facilitate the enlargement of the cerebral cortex during evolution, which is limited in Lissencephalic species, such as rodent (Figure.4). The size of ventricles expands in parallel with the expansion of cortical surface in Gyrencephalic mammals, while the ventricles shrink towards anterior side of the brain in mice (Paredes *et al*, 2016). This is in line with the concept that the ependymogenesis occur dominantly in the ventral telencephalon during mouse brain development. While the formation of an ependymal layer (highlighted by S100b staining in Figure.4) is limited to ventricular SVZ (V-SVZ) where the adult neurogenesis takes place in mice, a mature ependymal layer develops also in the dorsal telencephalon, or cortex, even in the posterior regions as exemplified on ferret tissue sections in Figure.4. Thus, our study

proposes that the human- and ferret-enriched tRG contributes to the ependyma formation, thereby allowing the expansion of the ventricles and the cerebral cortex in Gyrencephalic species.

By shedding light on the cellular events that drive brain expansion, our research contributes to the broader understanding of the adaptive advantages and functional implications of Gyrencephaly across mammalian species.

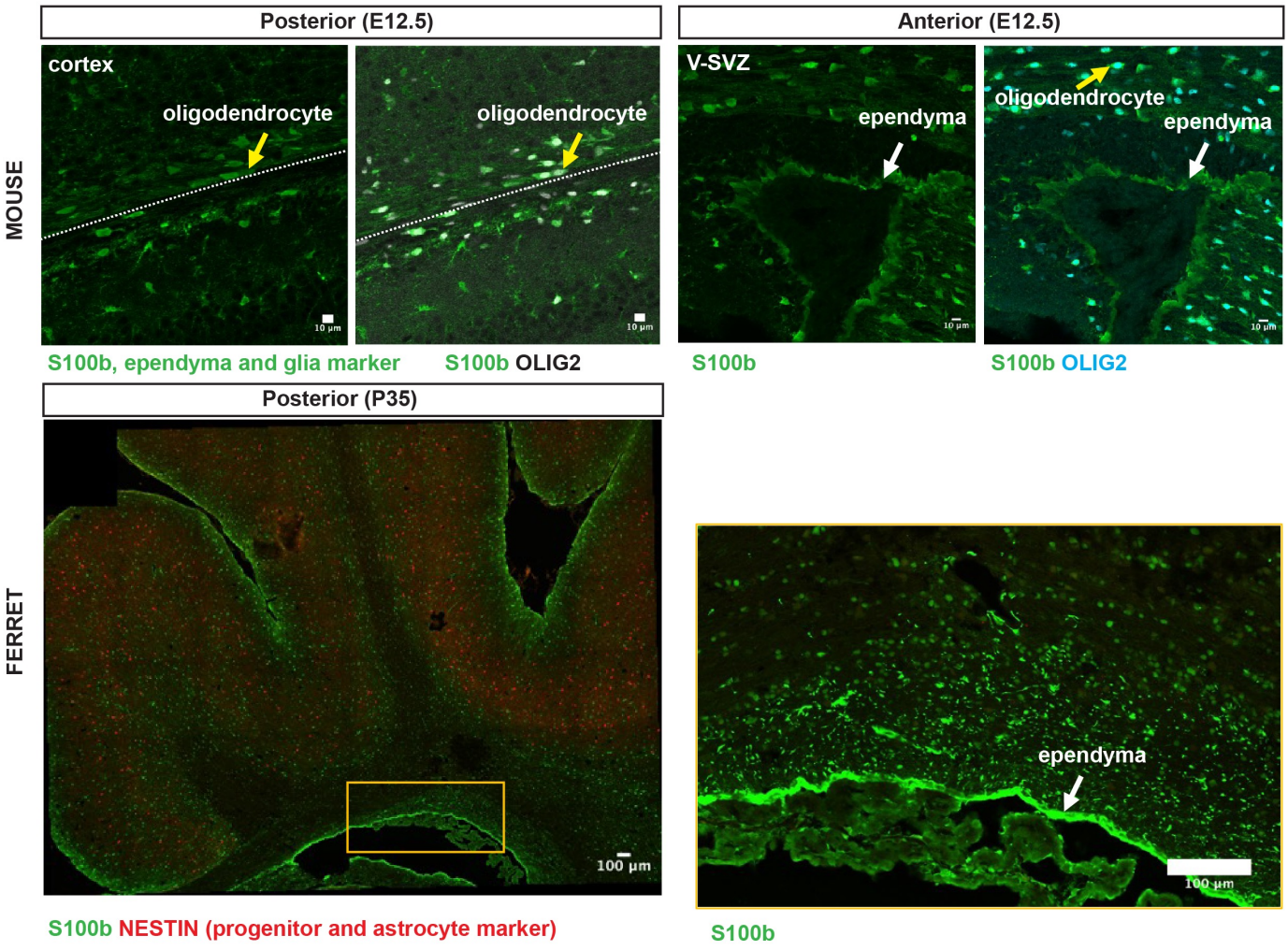

Figure 4. An expansion of ventricles with an ependymal layer in Gyrencephalic species. Immunostaining of S100b, an ependymal cell marker, on post-natal brain sections were compared between mice (Lissencephalic) and ferrets (Gyrencephalic), at P12.5 in mice, P35 in ferrets. Sections from the posterior (top left) or anterior (top right) regions of the brain are shown to represent the lack of an ependymal layer on the posterior side of mouse brain, while the corresponding brain region forms an ependymal layer.

4.3. Conserved diversity and temporal trajectory in human and ferret NPC.

Surprisingly, despite the considerable difference in timescale between human and ferret brain development, our research unveiled a conserved diversity and temporal trajectory in neural

progenitor cells between these species. This finding suggests fundamental similarities in the underlying mechanisms that govern cortical development in Gyrencephalic mammals. Understanding these conserved aspects may pave the way for cross-species comparisons and help bridge the knowledge gap between different models, advancing our comprehension of the fundamental principles governing brain formation in diverse mammalian species.

4.4. Prediction of tRG function in humans.

Through *in silico* and *in vivo* analyses, we predicted that tRGs in humans, similar to their counterparts in ferrets, likely acquire both ependymal and astrogenic fates during cortical development. This prediction is based on the comparison between human and ferret transcriptome datasets, highlighting commonalities in the molecular signatures of these neural progenitor cell subtypes. If confirmed, this insight would significantly contribute to our understanding of human brain development and the formation of adult ventricles, providing a basis for further research on neurogenesis and its relevance to brain function and health.

4.5. Future directions

In this PhD study, we failed to take advantage of *in vivo* fate tracing by specifically labeling tRG cells or their progenies. This might be due to a potential inaccessibility of *CRYAB* loci, the major target gene of ours to label tRG, to our guide RNAs, or a likely quiescent state of tRG cells during late embryonic and early postnatal stages. Using other markers to label tRG might overcome this issue in the future studies.

Furthermore, tRG cells seem to fail to form in human organoids, suggesting a requirement of external cues that may induce BMP signaling. For example, cerebrospinal fluid or choroid plexus might provide important cues to vRG *in vivo*. Improving organoid culture conditions is thus required to study the mechanisms of formation and differentiation of tRG, and to validate our suggestions based on ferret studies.

Moreover, our observation of a transformation of the VZ with a nuclear alignment might provide insights into the mechanisms how tRG differentiate into ependymal cells in the cortex. Future studies dissecting the molecular and cellular properties of these aligning cells by single cell isolation methods might provide deeper insights in the potential relationship between nuclear alignment and ependymal differentiation.

Taken together, future research directions may involve investigating the properties and functions of tRGs in ferrets to further improve our understanding of the factors influencing formation of tRG and its fates. Additionally, the potential therapeutic implications of these findings could be explored to address neurological disorders related to cortical development abnormalities.

The identification of tRG cells in different species may open new avenues of research into potential therapeutic targets for neurological disorders that involve abnormalities in cortical development. As we uncover more about the neural progenitor cell diversity and their roles, future studies can build upon this foundation, advancing our knowledge of brain development and its relevance to human health and cognition.

4.6. Conclusion

This PhD study on the development of the cerebral cortex in Gyrencephalic mammals, with a focus on ferrets as a model, has provided insights into the diversity and temporal trajectory of neural progenitor cells (NPC). The identification of truncated radial glia (tRG) in ferrets, a previously described but poorly understood NPC subtype in humans, has opened new avenues for

understanding the fundamental processes governing brain formation, such as their role and significance in corticogenesis. The prediction that tRGs in humans may acquire both ependymal and astrogenic fates based on transcriptome comparisons with ferrets provides valuable insights into human brain development and ventricle formation. These findings contribute to the architectural basis for comprehending the functional significance of Gyrencephaly across species.

By unraveling the mechanisms underlying the formation of the cerebral cortex and the roles of different neural progenitor cell subtypes, this research has implications beyond the specific study of ferrets. The findings may pave the way for cross-species comparisons and facilitate advancements in neuroscience, developmental biology, and evolutionary biology.

BIBLIOGRAPHY

A.J. J, M. D-P, M.M. G, P. F-L & J.-M. P-F (2014) Structure and function of the ependymal barrier and diseases associated with ependyma disruption. *Tissue Barriers* 2: 1–14

Arlotta P, Molyneaux BJ, Chen J, Inoue J, Kominami R & MacKlis JD (2005) Neuronal subtype-specific genes that control corticospinal motor neuron development in vivo. *Neuron* 45: 207–221

Asuka M, May T, C. YA, S. KS, Mami U, Masaharu O & Tomomi S (2013) BTBD3 Controls Dendrite Orientation Toward Active Axons in Mammalian Neocortex. *Science (80-)* 342(6162): 1114–1118

Betizeau M, Cortay V, Patti D, Pfister S, Gautier E, Bellemin-Ménard A, Afanassieff M, Huissoud C, Douglas RJ, Kennedy H, *et al* (2013) Precursor diversity and complexity of lineage relationships in the outer subventricular zone of the primate. *Neuron* 80: 442–457

Bhaduri A, Andrews MG, Mancia Leon W, Jung D, Shin D, Allen D, Jung D, Schmunk G, Haeussler M, Salma J, *et al* (2020) Cell stress in cortical organoids impairs molecular subtype specification. *Nature* 578(7793): 142–148

Bhaduri A, Sandoval-Espinosa C, Otero-Garcia M, Oh I, Yin R, Eze UC, Nowakowski TJ & Kriegstein AR (2021) An atlas of cortical arealization identifies dynamic molecular signatures. *Nature* 598(7879): 200–204

Borrell V (2010) In vivo gene delivery to the postnatal ferret cerebral cortex by DNA electroporation. *J Neurosci Methods* 186: 186–195

Borrell V & Reillo I (2012) Emerging roles of neural stem cells in cerebral cortex development and evolution. *Dev Neurobiol* 72: 955–971

Britanova O, Akopov S, Lukyanov S, Gruss P & Tarabykin V (2005) Novel transcription factor Satb2 interacts with matrix attachment region DNA elements in a tissue-specific manner and demonstrates cell-type-dependent expression in the developing mouse CNS. *Eur J Neurosci* 21: 658–668

DeAzevedo LC, Fallet C, Moura-Neto V, Daumas-Duport C, Hedin-Pereira C & Lent R (2003) Cortical radial glial cells in human fetuses: Depth-correlated transformation into astrocytes. *J Neurobiol* 55(3): 288–298

Dehay C, Kennedy H & Kosik KS (2015) The Outer Subventricular Zone and Primate-Specific Cortical Complexification. *Neuron* 85: 683–694

Dicke U & Roth G (2016) Neuronal factors determining high intelligence. *Philos Trans R Soc B Biol Sci* 371

Eiraku M, Watanabe K, Matsuo-Takasaki M, Kawada M, Yonemura S, Matsumura M, Wataya T, Nishiyama A, Muguruma K & Sasai Y (2008) Self-organized formation of polarized cortical tissues from ESCs and its active manipulation by extrinsic signals. *Cell Stem Cell* 3: 519–532

Fernández V, Llinares-Benadero C & Borrell V (2016) Cerebral cortex expansion and folding: what have we learned? *EMBO J* 35: 1021–1044

Fietz SA, Kelava I, Vogt J, Wilsch-Bräuninger M, Stenzel D, Fish JL, Corbeil D, Riehn A, Distler W, Nitsch R, *et al* (2010) OSVZ progenitors of human and ferret neocortex are epithelial-like and expand by integrin signaling. *Nat Neurosci* 13(6): 690–699

Frantz GD & McConnell SK (1996) Restriction of late cerebral cortical progenitors to an upper-layer fate. *Neuron* 17: 55–61

Fujita I, Shitamukai A, Kusumoto F, Mase S, Suetsugu T, Omori A, Kato K, Abe T, Shioi G,

Konno D, *et al* (2020) Endfoot regeneration restricts radial glial state and prevents translocation into the outer subventricular zone in early mammalian brain development. *Nat Cell Biol* 22: 26–37

Gertz CC, Lui JH, LaMonica BE, Wang X & Kriegstein AR (2014) Diverse Behaviors of Outer Radial Glia in Developing Ferret and Human Cortex. *J Neurosci* 34: 2559–2570

Gilardi C & Kalebic N (2021) The Ferret as a Model System for Neocortex Development and Evolution. *Front Cell Dev Biol* 9: 1004

Hansen D V., Lui JH, Parker PRL & Kriegstein AR (2010) Neurogenic radial glia in the outer subventricular zone of human neocortex. *Nat 2010 4647288* 464: 554–561

Haug H (1987) Brain sizes, surfaces, and neuronal sizes of the cortex cerebri: a stereological investigation of man and his variability and a comparison with some mammals (primates, whales, marsupials, insectivores, and one elephant). *Am J Anat* 180: 126–142

Herculano-Houzel S, Mota B & Lent R (2006) Cellular scaling rules for rodent brains. *Proc Natl Acad Sci U S A* 103: 12138–12143

Herring CA, Simmons RK, Freytag S, Poppe D, Moffet JJD, Pflueger J, Buckberry S, Vargas-Landin DB, Clément O, Echeverría EG, *et al* (2022) Human prefrontal cortex gene regulatory dynamics from gestation to adulthood at single-cell resolution. *Cell* 185: 4428-4447.e28

Huang W, Bhaduri A, Velmeshev D, Wang S, Wang L, Rottkamp CA, Alvarez-Buylla A, Rowitch DH & Kriegstein AR (2020) Origins and Proliferative States of Human Oligodendrocyte Precursor Cells. *Cell* 182(3): 594-608.e11

Jackson CA, Peduzzi JD & Hickey TL (1989) Visual Cortex Development in the Ferret. I. Genesis and Migration of Visual Cortical Neurons. *J Neurosci*: 1242–253

Johnson MB, Sun X, Kodani A, Borges-Monroy R, Girskis KM, Ryu SC, Wang PP, Patel K, Gonzalez DiM, Woo YM, *et al* (2018) Aspm knockout ferret reveals an evolutionary mechanism governing cerebral cortical size. *Nat 2018 5567701* 556: 370–375

Johnson MB, Wang PP, Atabay KD, Murphy EA, Doan RN, Hecht JL & Walsh CA (2015) Single-cell analysis reveals transcriptional heterogeneity of neural progenitors in human cortex. *Nat Neurosci* 18(5): 637–646

de Juan Romero C, Bruder C, Tomasello U, Sanz-Anquela JM & Borrell V (2015) Discrete domains of gene expression in germinal layers distinguish the development of gyrencephaly. *EMBO J* 34(14): 1859–1874

Kawasaki H, Iwai L & Tanno K (2012) Rapid and efficient genetic manipulation of gyrencephalic carnivores using in utero electroporation. *Mol Brain* 5: 1–7

Kawaue T, Shitamukai A, Nagasaka A, Tsunekawa Y, Shinoda T, Saito K, Terada R, Bilgic M, Miyata T, Matsuzaki F, *et al* (2019) Lzts1 controls both neuronal delamination and outer radial glial-like cell generation during mammalian cerebral development. *Nat Commun 2019 101* 10: 1–18

Kelly JB, Judge PW & Phillips DP (1986) Representation of the cochlea in primary auditory cortex of the ferret (Mustela putorius). *Hear Res* 24: 111–115

Kessaris N, Fogarty M, Iannarelli P, Grist M, Wegner M & Richardson WD (2006) Competing waves of oligodendrocytes in the forebrain and postnatal elimination of an embryonic lineage. *Nat Neurosci 2005 92* 9: 173–179

Konno D, Shioi G, Shitamukai A, Mori A, Kiyonari H, Miyata T & Matsuzaki F (2007) Neuroepithelial progenitors undergo LGN-dependent planar divisions to maintain self-renewability during mammalian neurogenesis. *Nat Cell Biol 2008 101* 10: 93–101

Liu J, Liu W, Yang L, Wu Q, Zhang H, Fang A, Li L, Xu X, Sun L, Zhang J, *et al* (2017) The Primate-Specific Gene TMEM14B Marks Outer Radial Glia Cells and Promotes Cortical Expansion and Folding. *Cell Stem Cell* 21(5): 635-649.e8

Mashiko H, Yoshida AC, Kikuchi SS, Niimi K, Takahashi E, Aruga J, Okano H & Shimogori T (2012) Comparative Anatomy of Marmoset and Mouse Cortex from Genomic Expression. *J Neurosci* 32: 5039–5053

McConnell SK (1985) Migration and Differentiation of Cerebral Cortical Neurons After Transplantation into the Brains of Ferrets. 229

McConnell SK (1988) Fates of visual cortical neurons in the ferret after isochronic and heterochronic transplantation. *J Neurosci* 8: 945–974

McInnes L, Healy J & Melville J (2018) UMAP: Uniform Manifold Approximation and Projection for Dimension Reduction. *arXiv* doi: 1802.

Nagao M, Ogata T, Sawada Y & Gotoh Y (2016) Zbtb20 promotes astrocytogenesis during neocortical development. *Nat Commun 2016 71* 7: 1–14

Noctor SC, Martinez-Cerdeño V, Ivic L & Kriegstein AR (2004) Cortical neurons arise in symmetric and asymmetric division zones and migrate through specific phases. *Nat Neurosci 2004 72* 7: 136–144

Noctor SC, Scholnicoff NJ & Juliano SL (1997) Histogenesis of Ferret Somatosensory Cortex. *J Comp Neurol* 387: 179–193

Nowakowski TJ, Bhaduri A, Pollen AA, Alvarado B, Mostajo-Radji MA, Di Lullo E, Haeussler M, Sandoval-Espinosa C, Liu SJ, Velmeshev D, *et al* (2017) Spatiotemporal gene expression trajectories reveal developmental hierarchies of the human cortex. *Science (80-)* 358(6368): 1318–1323

Nowakowski TJ, Pollen AA, Sandoval-Espinosa C & Kriegstein AR (2016) Transformation of the Radial Glia Scaffold Demarcates Two Stages of Human Cerebral Cortex Development. *Neuron* 91(6): 1219–1227

Ohtsuka T, Imayoshi I, Shimojo H, Nishi E, Kageyama R & McConnell SK (2006) Visualization of embryonic neural stem cells using Hes promoters in transgenic mice. *Mol Cell Neurosci* 31(1): 109–122

Okamoto M, Miyata T, Konno D, Ueda HR, Kasukawa T, Hashimoto M, Matsuzaki F & Kawaguchi A (2016) Cell-cycle-independent transitions in temporal identity of mammalian neural progenitor cells. *Nat Commun* 7:11349

Omiya H, Yamaguchi S, Watanabe T, Kuniya T, Harada Y, Kawaguchi D & Gotoh Y (2021) BMP signaling suppresses Gemc1 expression and ependymal differentiation of mouse telencephalic progenitors. *Sci Reports 2021 111* 11: 1–14

Paredes MF, Sorrells SF, Garcia-Verdugo JM & Alvarez-Buylla A (2016) Brain Size and Limits to Adult Neurogenesis. *J Comp Neurol* 524: 646

Polioudakis D, de la Torre-Ubieta L, Langerman J, Elkins AG, Shi X, Stein JL, Vuong CK, Nichterwitz S, Gevorgian M, Opland CK, *et al* (2019) A Single-Cell Transcriptomic Atlas of Human Neocortical Development during Mid-gestation. *Neuron* 103(5): 785-801.e8

Pollen AA, Nowakowski TJ, Chen J, Retallack H, Sandoval-Espinosa C, Nicholas CR, Shuga J, Liu SJ, Oldham MC, Diaz A, *et al* (2015) Molecular Identity of Human Outer Radial Glia during Cortical Development. *Cell* 163(1): 55–67

Poluch S & Juliano SL (2015) Fine-tuning of neurogenesis is essential for the evolutionary expansion of the cerebral cortex. *Cereb Cortex* 25: 346–364

Qiu X, Mao Q, Tang Y, Wang L, Chawla R, Pliner HA & Trapnell C (2017) Reversed graph

embedding resolves complex single-cell trajectories. *Nat Methods* 14: 979–982
Rash BG, Duque A, Morozov YM, Arellano JI, Micali N & Rakic P (2019a) Gliogenesis in the outer subventricular zone promotes enlargement and gyrification of the primate cerebrum. *Proc Natl Acad Sci* 116(14): 7089 LP – 7094
Rash BG, Duque A, Morozov YM, Arellano JI, Micali N & Rakic P (2019b) Gliogenesis in the outer subventricular zone promotes enlargement and gyrification of the primate cerebrum. *Proc Natl Acad Sci* 116(14)
Reillo I & Borrell V (2012) Germinal Zones in the Developing Cerebral Cortex of Ferret: Ontogeny, Cell Cycle Kinetics, and Diversity of Progenitors. *Cereb Cortex* 22: 2039–2054
Reillo I, De Juan Romero C, García-Cabezas MÁ & Borrell V (2011) A role for intermediate radial glia in the tangential expansion of the mammalian cerebral cortex. *Cereb Cortex* 21: 1674–1694
Roth G (2015) Convergent evolution of complex brains and high intelligence. *Philos Trans R Soc B Biol Sci* 370
Schindelin J, Arganda-Carreras I, Frise E, Kaynig V, Longair M, Pietzsch T, Preibisch S, Rueden C, Saalfeld S, Schmid B, *et al* (2012) Fiji: an open-source platform for biological-image analysis. *Nat Methods 2012 97* 9: 676–682
Shitamukai A, Konno D & Matsuzaki F (2011) Oblique radial glial divisions in the developing mouse neocortex induce self-renewing progenitors outside the germinal zone that resemble primate outer subventricular zone progenitors. *J Neurosci* 31: 3683–3695
Smart IHM, Dehay C, Giroud P, Berland M & Kennedy H (2002) Unique Morphological Features of the Proliferative Zones and Postmitotic Compartments of the Neural Epithelium Giving Rise to Striate and Extrastriate Cortex in the Monkey. *Cereb Cortex* 12(1): 37–53
Stuart T, Butler A, Hoffman P, Hafemeister C, Papalexi E, Mauck WM, Hao Y, Stoeckius M, Smibert P & Satija R (2019) Comprehensive Integration of Single-Cell Data. *Cell* 177(7): 1888-1902.e21
Szemes M, Gyorgy A, Paweletz C, Dobi A & Agoston D V. (2006) Isolation and characterization of SATB2, a novel AT-rich DNA binding protein expressed in development- and cell-specific manner in the rat brain. *Neurochem Res* 31: 237–246
Taverna E, Götz M & Huttner WB (2014) The Cell Biology of Neurogenesis: Toward an Understanding of the Development and Evolution of the Neocortex. *https://doi.org/101146/annurev-cellbio-101011-155801* 30: 465–502
Telley L, Agirman G, Prados J, Amberg N, Fièvre S, Oberst P, Bartolini G, Vitali I, Cadilhac C, Hippenmeyer S, *et al* (2019) Temporal patterning of apical progenitors and their daughter neurons in the developing neocortex. *Science* 364
Tonchev AB, Tuoc TC, Rosenthal EH, Studer M & Stoykova A (2016) Zbtb20 modulates the sequential generation of neuronal layers in developing cortex. *Mol Brain* 9: 1–15
Trapnell C, Cacchiarelli D, Grimsby J, Pokharel P, Li S, Morse M, Lennon NJ, Livak KJ, Mikkelsen TS & Rinn JL (2014) The dynamics and regulators of cell fate decisions are revealed by pseudotemporal ordering of single cells. *Nat Biotechnol* 32(4): 381–386
Tsunekawa Y, Terhune RK, Fujita I, Shitamukai A, Suetsugu T & Matsuzaki F (2016) Developing a de novo targeted knock-in method based on in utero electroporation into the mammalian brain. *Development* 143: 3216–3222
Wu Q, Shichino Y, Abe T, Suetsugu T, Omori A, Kiyonari H, Iwasaki S & Matsuzaki F (2022) Selective translation of epigenetic modifiers affects the temporal pattern and differentiation of neural stem cells. *Nat Commun 2022 131* 13: 1–18

Yamamoto S, Yamashita A, Arakaki N, Nemoto H & Yamazaki T (2014) Prevention of aberrant protein aggregation by anchoring the molecular chaperone αB-crystallin to the endoplasmic reticulum. *Biochem Biophys Res Commun* 455: 241–245

Yusa K, Zhou L, Li MA, Bradley A & Craig NL (2011) A hyperactive piggyBac transposase for mammalian applications. *Proc Natl Acad Sci U S A* 108: 1531–1536

Zheng K, Wang C, Yang J, Huang H, Zhao X, Zhang Z & Qiu M (2018) Molecular and Genetic Evidence for the PDGFRα-Independent Population of Oligodendrocyte Progenitor Cells in the Developing Mouse Brain. *J Neurosci* 38: 9505–9513

Zhong S, Zhang S, Fan X, Wu Q, Yan L, Dong J, Zhang H, Li L, Sun L, Pan N, *et al* (2018) A single-cell RNA-seq survey of the developmental landscape of the human prefrontal cortex. *Nature* 555(7697): 524–528

ACKNOWLEDGEMENT

This thesis is based on material contained in the following scholarly paper.

Merve Bilgic, Quan Wu, Taeko Suetsugu, Atsunori Shitamukai, Yuji Tsunekawa, Tomomi Shimogori, Mitsutaka Kadota, Osamu Nishimura, Shigehiro Kuraku, Hiroshi Kiyonari, Fumio Matsuzaki. Truncated radial glia as a common precursor in the late corticogenesis of gyrencephalic mammals. eLife, 2023. https://doi.org/10.7554/eLife.91406.2

I would like to express my deepest gratitude to the following individuals and groups whose unwavering support and guidance were instrumental throughout my arduous seven-year journey in pursuit of my PhD: First, I dedicate this thesis to my beloved grandmother, whose love and encouragement had been an unwavering source of inspiration. I am profoundly thankful to my family for their belief in me and the enduring love that formed the bedrock of my determination.

I extend my deepest appreciation to Fumio Matsuzaki, my supervisor, whose invaluable mentorship and for his invaluable support guided me through every phase of this transformative journey. I extend my gratitude to the members of the Matsuzaki lab, who welcomed me with open arms during the early stages of my time in Japan and patiently shared their scientific knowledge. Special thanks to Wu Quan for guiding me in single-cell RNA-sequencing analyses, Suetsugu-san for her constant assistance in ferret experiments, and Tsunekawa-san for teaching me his Crispr-Cas9 approach. I cherish the moments of camaraderie during our regular coffee breaks with Omori-san, Yoshida-san, Kamatani-san, Suetsugu-san, and Ishigai-san. A special recognition goes to Tomomi Shimogori for her invaluable guidance in in situ hybridization, a skill critical to the success of my research. I am thankful to Kuraku-san and Nishimura-san, whose pivotal role in generating new gene models for ferrets significantly advanced this project. I am indebted to Kiyonari-san for his care of the ferrets involved in my research.

I would like to express my heartfelt appreciation to the Riken Girls Health Club for their mental support during challenging times and for enhancing the warm memories of life in Kobe.

I extend my sincere thanks to Yusuke Kishi for his continuous support and for granting me the autonomy to pursue my aging project, even as I continued my tenure in his lab without completing my PhD. I am profoundly grateful to Yukiko Gotoh for motivating me to aim higher and for advocating women in academia.

Furthermore, I want to express my heartfelt gratitude to Fumiya Kusumoto who has been my lifetime partner and unwavering source of support, both in my personal life and in my academic pursuits.

Last but not least, I extend my heartfelt thanks to all my friends who stood by me, including Tanita, Hanae, Hou-chan and many others providing invaluable mental support and helping me strike a balance between work and life. Your contributions have been indispensable to the completion of this PhD journey, and for that, I am deeply grateful.